AD 295 089

63-2-3

U. S. ARMY
TRANSPORTATION RESEARCH COMMAND
FORT EUSTIS, VIRGINIA

TCREC TECHNICAL REPORT 62-44

A METHOD FOR COMPUTING ROTARY WING AIRLOAD DISTRIBUTION IN FORWARD FLIGHT

Task 9R38-01-019-04

Contract DA 44-177-TC-698

November 1962

prepared by:

CORNELL AERONAUTICAL LABORATORY, INC.
Buffalo, New York

DISCLAIMER NOTICE

When Government drawings, specification, or other data are used for any purpose other than in connection with a definitely related Government procurement operation the United States Government thereby incurs no responsibility nor any obligation whatsoever; and the fact that the Government may have formulated, furnished, or in any way supplied the said drawings, specifications, or other data is not to be regarded by implication or otherwise as in any manner licensing the holder or any other person or corporation, or conveying any rights or permission, to manufacture, use, or sell any patented invention that may in any way be related thereto.

* * *

ASTIA AVAILABILITY NOTICE

Qualified requesters may obtain copies of this report from

Armed Services Technical Information Agency
Arlington Hall Station
Arlington 12, Virginia

* * *

This report has been released to the Office of Technical Services, U. S. Department of Commerce, Washington 25, D. C., for sale to the general public.

* * *

The information contained herein will not be used for advertising purposes.

* * *

The findings and recommendations contained in this report are those of the contractor and do not necessarily reflect the views of the U. S. Army Mobility Command, the U. S. Army Materiel Command, or the Department of the Army.

HEADQUARTERS
U. S. ARMY TRANSPORTATION RESEARCH COMMAND
Fort Eustis, Virginia

This report has been reviewed by the U. S. Army Transportation Research Command and is considered to be technically sound. The report is published for the exchange of information and the stimulation of ideas.

FOR THE COMMANDER:

KENNETH B. ABEL
Captain TC
Adjutant

APPROVED BY:

JOHN E. YEATES
USATRECOM Project Engineer

Task 9R38-01-019-04

Contract DA 44-177-TC-698

November 1962

A METHOD FOR COMPUTING ROTARY WING AIRLOAD DISTRIBUTIONS IN FORWARD FLIGHT

CAL REPORT BB-1495-S-1

Prepared by

Cornell Aeronautical Laboratory, Inc.
Buffalo, New York

for

U. S. Army Transportation Research Command
Fort Eustis, Virginia

FOREWORD

The technical effort reported herein was conducted at Cornell Aeronautical Laboratory, Inc., by Messrs. Raymond A. Piziali and Frank A. DuWaldt during the period from September 1960 through April 1962. This program was sponsored by the U. S. Army Transportation Research Command, Fort Eustis, Virginia, and administered by Mr. J. Yeates.

Assistance and helpful criticisms were received from Messrs. J. G. McHugh and J. Yeates of TRECOM; Messrs. J. deTore, F. Burpo, B. Blankenship, and other personnel at Bell Helicopter Corporation; Messrs. D. Jenney of United Aircraft Research Laboratories and J. Rabbott of Sikorsky Helicopter; Messrs. F. Gustafson and J. Scheiman of NASA, Langley. Finally, thanks are due Mr. W. Targoff, formerly at Cornell Aeronautical Laboratory, for his encouragement and active participation in all aspects of the effort. The form in which the problem was cast and the method of solution stem directly from his collaboration.

TABLE OF CONTENTS

LIST OF FIGURES

LIST OF TABLES

NOMENCLATURE

a - Lift curve slope: $\partial C_l / \partial \alpha_e$

b - Blade semichord at each radial station.

h - "Effective" plunging velocity of the blade section; includes the component of the free stream velocity, V_f, normal to the local blade sections (i.e., the effects of the local blade slopes).

k - Subscript indicating position in the rotor disk.

l - Lift per unit span.

n - Number of radial bound vortex segments representing blades.

N - Number of equally-spaced azimuth positions at which the airloads are computed; must be multiple of the number of blades in the rotor.

P - The points of the rotor disk where the airloads are computed.

r - The radial coordinate of the rotor.

R - Blade radius.

V - Tangential velocity in tip-path-plane: $V = \Omega r + V_f \cos \alpha_T$

V_f - Free stream velocity due to rotor translation.

w_r - The induced velocity component normal to the tip-path-plane at the three-quarter-chord of the section.

α - Instantaneous geometric angle of attack with respect to the tip-path-plane.

$\hat{\alpha}$ - Stalling angle of attack for the blade sections.

α_e - Instantaneous effective angle of attack with respect to the tip-path-plane: $\alpha_e = \alpha - \dot{h}/V + w/V$.

α_T - Longitudinal tip-path-plane inclination with respect to the free stream velocity, V_f .

Γ - The unknown strength of the bound vortex segment representing the blade section.

μ - Advance ratio: $\mu = V_f \cos\alpha_T / \Omega R$.

ρ - Air density.

ψ - Azimuthal position.

Ω - Rotational speed of the rotor.

SUMMARY

This investigation is an initial effort to obtain a solution to the airloads problem for a rotating wing in steady-state translational flight. A sufficient amount of the wake detail was retained to enable accurate computation of the wake-induced velocities at the blade. The method of solution developed is numerical, utilizes high-speed digital computation, and is relatively simple to use.

Each blade is represented by a segmented lifting line and the shed and trailing vorticity distributions are represented by a continuous mesh of segmented vortex filaments originating at the instantaneous position of the blade. The wake of each blade of the rotor is different; these wakes change with the azimuth position of the blades to correspond to the instantaneous wake configuration for each azimuth position.

The method developed was used to compute the rotor airload distributions for the Bell HU-1A, the Sikorsky H-34, and an NASA model rotor in forward flight. The computed airloads were harmonically analyzed and the radial distribution of each harmonic compared with the measured distributions. In general, encouraging agreement is obtained in these comparisons. Effects of changing some of the parameters of the computation were investigated.

INTRODUCTION

The problem of predicting the aeroelastic response of rotating wings is generally recognized to be very difficult. The industry has had to rely on expensive empirical methods and past experience to design and develop these aircraft components.

It is believed that the investigation that is being reported herein can be put in its proper context by relating it to the continuing research program on helicopter dynamics that has been carried out for many years at Cornell Aeronautical Laboratory.

One of the earliest direct anticedents (initiated in 1945) of the current effort is the "H-5 Variable Stiffness Blade Program", Refs. 4 - 21. That study was initially aimed at determining if rotor blade structural stiffness was an important factor in the blade fatigue life. Early in this program it was found from strain gage measurements (made in flight) that higher harmonic order bending moments of large amplitude existed when a multiple of the rotor rpm was near the frequency of the second or third natural bending mode. Thereafter, emphasis of the program was concentrated on investigation and evaluation of the resonance effects. It was postulated that the forcing functions exciting the bending modes of the blades (and the fuselage modes) arose from aerodynamic forces whose existence could be explained only on the basis of nonuniform inflow

velocities. Comparison of generalized forces derived from measured strain data with generalized forces computed from downwash velocities based on Mangler's analysis (Ref. 22) tended to confirm this hypothesis. It was also noted that Mangler's analysis was not sufficiently refined to permit adequate blade stress calculations.

Thus, The "H-5 Variable Stiffness Blade Program" resulted in the identification of the complex-induced velocity distribution as the aerodynamic part and the resonance conditions as the structural part of the rotor fatigue problem. A semiempirical approach based on the use of generalized forces obtained from strain measurements was recommended for analyzing rotors. It is believed that this approach is still used as a basis for the analysis of rotor stresses.

Recognition that the rotor bending stress problem was, in fact, an aeroelastic problem led to a more careful consideration of the possibilities of rotor flutter and, conversely, the possibilities for introducing couplings between blade modes that would alleviate stresses. Several studies characterized by analytical developments and corroborating experiments were made (Refs. 23 - 35). It was noted that fair agreement between theoretical and experimental flutter results was obtained for most hovering configurations but that, under certain conditions, a multiplicity of flutter modes was obtained which were not predicted. The multiplicity could not be accounted for on the basis of mass and elastic characteristics alone, and it was concluded that the wake strength and position associated with the blade flutter motions was a major

effect. In fact, the name "wake excited flutter" was applied to certain of the flutter modes that had frequencies which were nearly integer multiples of rotor speed. Further analytical work resulted in establishment of a two-dimensional unsteady aerodynamic theory for a hovering rotor (Ref. 28) that predicted the multiple flutter loops and further verification was obtained from additional flutter and response tests (Refs. 30 and 32). Forward flight flutter investigations (Refs. 34 and 35) were also initiated, although it was realized that no suitable unsteady aerodynamic theory was available for this flight regime.

The results reported herein can thus be viewed as a logical development in a history that started more than fifteen years ago. It began with the proper identification of the blade oscillatory stress problem and the development of an interim semiempirical solution. Then it proceeded through a systematic series of aeroelastic analyses and validating tests, which led logically to the present effort.

The aeroelastic problem can be thought of as consisting of two parts: the dynamic response, and the airloads. They are interdependent and related in that the airloads cause the dynamic response and, at the same time, depend on it. Much of the difficulty in obtaining an adequate solution to the aeroelastic problem is in the airloads part of the problem (specifically in obtaining an adequate aerodynamic representation of the blades and wake).

Any accurate method of computing the airloads must adequately predict

the wake-induced velocities at the blades because the airloads are strongly influenced by these velocities. However, because the vortical wake of the rotating wing is extremely complex and difficult to adequately represent mathematically, the practical solution of the aeroelastic problem has been delayed. Early attempts to solve this problem analytically were based on relatively drastic simplifications of the wake of the rotor to make them computationally feasible. The modern high-speed computing machines of today have made it possible to account for much more of the detail of the wake than has been possible in the past and thus permit an adequate aerodynamic representation of the blades and wake to be formulated which will enable accurate computation of the rotor airload distribution. The method of computing airloads developed in this investigation makes use of high-speed digital computation to retain much of the detail of the wake.

Measured motion and strain data were used in an effort to separate the airloads problem from the response problem and, thereby, permit concentration of effort in this investigation on the formulation of an adequate aerodynamic representation. It was found that separating the airloads and response in this manner was relatively unsatisfactory because known constraints are not satisfied (e.g., the first harmonic moment about the flap hinge should be zero). If the motions had been computed with the airloads instead of using the measured motions and separating the problem, these constraints would have been satisfied.

The method developed was used to compute the airload distribution for three flight conditions of an NASA wind tunnel model rotor (described in Refs. 1, 2 and 3), four flight conditions of the Bell HU-1A full-scale helicopter, and two flight conditions of the Sikorsky H-34 full-scale helicopter. The comparisons of some of these computed airloads with the corresponding measured airloads are presented and discussed in this report.

Sensitivity of the computed airloads to several of the parameters of the computation were investigated computationally, and the results are presented and discussed.

The Computational Model

It is assumed that the rotor is operating in steady-state flight. The generated wake and the airloads are, therefore, the same for each revolution of the blades, i.e., the form of the wake is periodic and the blades will "see" the same wake each time they are in the same azimuth position. It is also assumed that the effects of viscous dissipation in the wake can be neglected.

Each blade of the rotor is represented by a segmented lifting-line (bound vortex) located along the steady deflected position of the quarter-chord. The number of segments, n , and the length of each segment are arbitrary; they are each straight and of constant vortex strength. The lifting line is considered to advance in a stepwise manner through " N " equally-spaced azimuth positions.

In the wake, the shed and trailing vorticity distributions of each blade are represented by a mesh of segmented vortex filaments; each segment is straight and of constant vortex strength. The segmented trailing vortex filaments emanate from each of the end points of the lifting-line segments. The segmented shed vortex filaments intersect the trailing filaments in a manner such that the end points of both are coincident (Fig. 1).

The strengths, $d\Gamma/d\psi$, of the shed elements are equal to the change in strength of the bound vortex segments between successive azimuth stations and are deposited in the flow at each azimuth station of the bound vortex. The strengths, $d\Gamma/dr$, of the trailing vortex elements are equal to the differences in strengths of adjacent bound vortex segments and are deposited in the flow in a manner such that they connect the bound vortex end points to the shed vortex end points. The displacement time history of the wake elements is specified, but this specification is relatively unrestricted. Thus, in this method, any physically realistic distortion of the wake can be incorporated into the computation of the airloads.

The Simultaneous Equations

For each azimuth position, the airloads are computed at the mid-points of the lifting-line segments. Thus, the airloads are computed at $(n)\cdot(N)$ points of the rotor disk. These points P_k of the disk are labeled as shown in the example of Fig. 2; subscript, k, refers to position in the disk. The expression for the lift per unit span, for a blade section at any point, P_k, of the disk, is

(1) $$l_k = \rho V_k \Gamma_k$$

where

(2) $$\Gamma_k = a_k b_k |V_k| \left(\alpha_k - \frac{h_k}{V_k} + \frac{w_k}{V_k} \right)$$

The quantity in parentheses is the instantaneous "effective" angle-of-attack at the three-quarter-chord point, where α_k is the instantaneous geometric angle-of-attack with respect to the tip-path-plane, $\dot{h}_k$ the "effective" plunging velocity with respect to the tip-path-plane, and w_{Γ_k} the velocity component normal to the tip-path-plane induced by all the wake vorticity and the bound vorticity of other blades. The strengths Γ_k of the bound vortex elements are considered to be the unknowns for the method of solution developed.

The velocity component in a given direction induced at a point by an arbitrarily oriented straight vortex filament of constant strength is given by the Biot-Savart law as:

$$q_f = f\gamma \tag{3}$$

where γ is the constant vortex strength of the filament, and the coefficient f is a function only of the coordinates of the point where the velocity is being computed and the coordinates of the vortex filament end points. The velocity, w_{Γ_k}, of Eq. 2 can be computed by summing the contributions (given by Eq. 3) of each individual vortex element of the blades and wake as indicated by Eq. 4.

$$w_{\Gamma_k} = \sum_{\text{Wake}} f\gamma + \sum_{\text{Blades}} f\Gamma \tag{4}$$

However, each wake vortex element strength γ of Eq. 4 is just the difference in strength of two of the unknown bound vortex segment strengths, Γ_k (i.e., $\gamma = \Gamma_a - \Gamma_b$, where a and b are two values of the disk position subscript, k). These γ relationships are depicted in Fig. 1 relative to a

point P_k of the rotor disk. If these differences are substituted for the γ, Eq. 4 can be expanded and the unknown Γ_k grouped and factored out. Thus, the w_k can be expressed as

$$w_k = \sum_{i=1}^{nN} \sigma_{ki} \Gamma_i \tag{5}$$

In Eq. 5, the Γ_i are the unknown bound vortex strengths and each σ_{ki} is the sum of all the coefficients f of a common Γ_i in Eq. 4. By substituting the w_k given by Eq. 5 in Eq. 2 and letting $I_k = a_k b_k (V_k \alpha_k - h_k)$, the following expression for Γ_k is obtained:

$$\Gamma_k = \frac{|V_k|}{V_k} \left[I_k + a_k b_k \sum_{i=1}^{nN} \sigma_{ki} \Gamma_i \right] \tag{6}$$

A set of linear simultaneous nonhomogeneous equations with constant coefficients is obtained when Eq. 6 is written for each point, P_k, of the rotor disk at which the airload is to be computed. Thus, the airloads problem is reduced to obtaining the solution to this set of equations for which the unknowns are the $(n) \cdot (N)$ bound vortex strengths Γ_k.

Solution of the Equations

An iterative procedure which is described below is used to solve the set of simultaneous equations. First, Eq. 6, the general equation of the set, is rearranged and put in the following form with the unknowns on the right side of the equation:

$$\bar{I}_k = \sum_{i=1}^{nN} \bar{\sigma}_{ki}\,\Gamma_i \tag{7}$$

where

$$\bar{\sigma}_{ki} = a_k b_k \sigma_{ki} \Big/ \left(a_k b_k \sigma_{kk} - |V_k|/V_k\right)$$

$$\bar{\sigma}_{kk} = 1.0$$

$$\bar{I}_k = -I_k \Big/ \left(a_k b_k \sigma_{kk} - |V_k|/V_k\right)$$

Thus, the set of equations to be solved is:

$$\begin{aligned}
\bar{I}_1 &= (1.0)\Gamma_1 + \bar{\sigma}_{1,2}\Gamma_2 + \bar{\sigma}_{1,3}\Gamma_3 + \cdots + \bar{\sigma}_{1,i}\Gamma_i + \cdots + \bar{\sigma}_{1,nN}\Gamma_{nN} \\
\bar{I}_2 &= \bar{\sigma}_{2,1}\Gamma_1 + (1.0)\Gamma_2 + \bar{\sigma}_{2,3}\Gamma_3 + \cdots + \bar{\sigma}_{2,i}\Gamma_i + \cdots + \bar{\sigma}_{2,nN}\Gamma_{nN} \\
\bar{I}_3 &= \bar{\sigma}_{3,1}\Gamma_1 + \bar{\sigma}_{3,2}\Gamma_2 + (1.0)\Gamma_3 + \cdots + \bar{\sigma}_{3,i}\Gamma_i + \cdots + \bar{\sigma}_{3,nN}\Gamma_{nN} \\
&\vdots \\
\bar{I}_k &= \bar{\sigma}_{k,1}\Gamma_1 + \bar{\sigma}_{k,2}\Gamma_2 + \bar{\sigma}_{k,3}\Gamma_3 + \cdots + (1.0)\Gamma_k + \cdots + \bar{\sigma}_{k,i}\Gamma_i + \cdots + \bar{\sigma}_{k,nN}\Gamma_{nN} \\
&\vdots \\
\bar{I}_{nN} &= \bar{\sigma}_{nN,1}\Gamma_1 + \bar{\sigma}_{nN,2}\Gamma_2 + \bar{\sigma}_{nN,3}\Gamma_3 + \cdots + \bar{\sigma}_{nN,i}\Gamma_i + \cdots + (1.0)\Gamma_{nN}
\end{aligned} \tag{8}$$

For the first iteration only, the set of equations is assumed to be completely diagonalized (i.e., the off-diagonal $\bar{\sigma}$'s are assumed equal to zero); thus, from the first iteration, the $\Gamma_k^{(1)}$ are equal to the $\bar{I}_k$ where the superscript represents the iteration number. The second and succeeding approximations to

the Γ_k are obtained by an iterative procedure governed by the following equation which is solved in succession for $\Gamma_k^{(j)}$ with $k = 1, 2, 3, \cdots n \cdot N$:

$$(9) \quad \Gamma_k^{(j)} = \bar{I}_k - \sum_{\lambda=1}^{k-1} \bar{\bar{a}}_{k,\lambda} \Gamma_\lambda^{(j)} - \sum_{\lambda=k+1}^{n \cdot N} \bar{\bar{a}}_{k,\lambda} \Gamma_\lambda^{(j-1)}$$

The following is a brief word description of the iterative procedure governed by Eq. 9:

Beginning with the first equation in the set, each is solved in succession for the unknown Γ on the diagonal by using for all Γ's to the left of the diagonal the approximations to Γ thus far obtained in the present (j^{th}) iteration (i.e., the $\Gamma_{\lambda<k}^{(j)}$ where k represents the equation number); and for all the Γ's to the right of the diagonal, the approximate values obtained in previous $\left((j-1)^{th}\right)$ iteration (i.e., the $\Gamma_{\lambda>k}^{(j-1)}$). In Eq. 9, the terms to the left of the diagonal are represented by the first summation and those to the right by the second summation.

Discussion

The following are the major assumptions which have been made in developing the computational model and procedure and have made it possible to reduce the airloads problem to a set of simultaneous equations:

1. The rotor has been in steady flight long enough for the wake to become periodic, i.e., the generated wake is the same for each revolution of the blades.

2. The effects of viscous dissipation on wake vortex strengths can be neglected.

3. The blades can be represented by lifting lines.

4. The trailing and shed vorticity distributions of the wake can be represented by a mesh of segmented vortex filaments.

5. The displacement time history of these wake elements is specified.

The framework of the method has been made sufficiently general to permit incorporation of the effects of the following:

1. Number of blades
2. Finite span
3. Planform taper
4. Twist
5. Variable lift curve slope
   a. Mach number
   b. Reynolds number
6. Stall and reversed flow
7. Blade elastic deformations
8. Control system deformation
9. Blade rigid body motions
10. Mutual interference of rotors

Stall effects are introduced into the computations during the solution of the simultaneous equations by determining the effective angle of attack and limiting the Γ_k accordingly. For the computations which were made, the lift coefficient was assumed to be constant and equal to its value at the stall angle for angles of attack greater than the stall angle. The limiting Γ_k (i.e., the stalled value of Γ_k) for these calculations were then computed from Eq. 6 by substituting the airfoil section stalling angle of attack $\hat{\alpha}$ for the effective angle of attack, $\left(\alpha_k - h_k/V_k + w_k/V_k\right)$; thus, the limiting Γ_k were computed from the following:

$$\hat{\Gamma}_k = a_k b_k |V_k| \hat{\alpha}$$

It is, however, possible within the present framework of the method to use more representative lift coefficient variations with angle of attack than the one chosen here. It should be noted that incorporating stall in this manner assumes that all of the stalled section lift is circulatory and there is, therefore, shed and trailing vortex elements in the wake whose strengths are determined by these stalled values of Γ_k .

In reality, when an airfoil section is stalled, the predominant part of the airload on the section may be noncirculatory and due to the separated flow. During the stalled condition, the vorticity introduced in the wake may be relatively small and of a considerably different nature than that of an unstalled section. Some indication of the magnitude of the separated flow forces

experienced is evident when the total measured airloads are examined. If the local dynamic pressure and measured airload are used to compute the corresponding normal force coefficient, it is found to be extremely large for some points of the rotor disk. These large "measured" normal force coefficients occur in regions of the rotor disk where the blades are supposedly stalled. These forces are analogous to the normal force on a flat plate at very large angles of attack.

Reversed flow effects are accounted for in the computation approximately in that the sign of the lift force and the sense of the bound, shed and trailing vorticity are always consistent with the local tangential velocity, V, and the "effective" relative angle-of-attack of the section as it approaches and passes through the region of reversed flow. However, for the computations which were performed, the wake remained attached to the bound vortex of the blade (although its position and orientation corresponded to the local inflow velocity) and the bound vortex remained at the quarter-chord while the blade approached and passed through the region of reversed flow. In reality, when a section is operating unstalled in reversed flow, the center of pressure is approximately at the three-quarter-chord and the bound vortex should be placed at that station and the induced velocity calculated at the quarter-chord.

Mach number (less than one) and Reynolds number effects can be accounted for as variations of the lift curve slope of the local blade sections. For a given rotor and operating conditions, the Mach number and Reynolds number distributions over the rotor disk are fixed (known); thus, these effects can be incorporated into the computations by introducing the proper distribution of lift curve slope over the disk.

Parameters of the Computations

A computational investigation was made to determine the sensitivity of the computed airloads to several "parameters" of the method: They are, the number of revolutions of wake used, the number of radial segments used to represent the blades, and the distortion of the wake. This computational investigation was made for the NASA model rotor at an advance ratio of 0.15. Experimental azimuthal load distributions are shown on Figure 3 for this case.

It was found for this rotor and operating condition that truncating the wake at three revolutions put the wake termination approximately one-and-one-half rotor diameters away from the rotor disk and accounted for practically all of the wake-induced velocities; extending the wake to five revolutions only resulted in a maximum change of two percent in the magnitudes of the lowest harmonics of the computed airloads. This was expected because the additional wake is relatively far from the rotor and the induced velocities due to it are relatively uniform over the disk; whereas, the induced velocity distribution due to the nearer or most recent wake has a considerable variation over the rotor disk and is the primary source of the higher harmonic components of the airloads. It is believed that the amount of wake (expressed in terms of a corresponding number of rotor revolutions) which is necessary to adequately predict the induced velocities at the blades will depend on the given rotor and its flight condition.

For this same rotor and operating condition, the sensitivity of the computed airloads to the number of radial segments used to represent the blades was investigated by computing the airloads for both five and nine radial

segments. A comparison of the results of these computations is presented in Figure 4. At this time it is not possible to draw any specific conclusions from these results other than to note that a change in the number of radial segments from five to nine for this rotor and operating condition can have some effect on the airloads.

For both the five and nine radial segment computations, the same first harmonic flapping motions were used. However, the constraint of zero moment about the flapping hinge due to the first harmonic component of the airload is not satisfied for either of these cases; this constraint arises from the flapping equation of motion. For a proper comparison of the airloads computed with five and nine radial segments, this flapping moment constraint should be applied in each case. This could be done by including the flapping equations of motion in the set of equations and solving simultaneously for the airloads and the flapping motion.

Sensitivity of the computed airloads to distortion of the wake was also investigated for this rotor and operating condition by using several relatively arbitrary distortions. The simplest wake distortion used corresponded to a radial distribution of the zeroth harmonic component of the inflow velocity distribution in the nonrotating system. The most elaborate corresponded to the use of harmonics of this velocity distribution through the fourth with magnitudes up to thirty percent of the zeroth harmonic. Common to each of these wake distortions was the assumption that the velocity of transport of each wake element end point was constant with time. The velocity used

for each segment end point was taken to be the vector sum of the rotor translational velocity and the component of inflow velocity normal to the rotor disk (tip-path-plane) at the point of the disk where the segment end point originated (i.e., the end points were assumed to retain their initial velocities). Thus, at any instant of time, the wake element end points defined a distorted helical surface. The wake of each blade, at any instant of time, is different and changes with azimuth position to correspond to the instantaneous wake configuration for that azimuth position.

It was found that the computed airloads were sensitive to these distortions of the wake for this flight condition of this rotor. It should be noted here, again, that the distortions of the wake (i.e., displacement time history of the wake) which can be used in this method of computing rotor airloads are relatively unrestricted. There remains, however, the question as to what displacement time history should be used for a particular rotor and operating condition. Using a uniform inflow distribution, determined from momentum considerations, to define the time history, has resulted in computed airloads which agree quite well with the measured airloads. This is evidently a good first approximation for the conditions analyzed; therefore, the addition of a few of the lower harmonic variations of the inflow distribution (in the nonrotating system) may be all that is necessary to adequately define the wake displacement time history. It is possible, by making a few modifications to the present method, to compute in addition the periodic induced velocity distribution in the nonrotating system.

The method as developed for computing the airload distribution has been programmed (in FORTRAN for the IBM 704) such that it is relatively simple to use. The printed output obtained from the program includes the following distributions given as functions of the radial and azimuthal position in the disk.

1. Airload on the blades
2. Strength of the bound vorticity
3. Effective angle of attack
4. Stalled angles of attack
5. Induced velocity at blade
6. Induced drag

Items 1, 2, 5 and 6 are also harmonically analyzed and the Fourier sine and cosine coefficients printed out.

MEASURED RESULTS USED FOR CORRELATION

Source

The measured airloads and motions which were used to test the adequacy of the computational model and procedures were selected from three sources: full-scale flight tests of the HU-1A helicopter by Bell Helicopter Corporation (Ref. 36), wind tunnel tests of a model rotor by the NASA (Refs. 1 - 3), and full-scale flight tests of the H-34 helicopter by the NASA (Ref. 37). The HU-1A has a two-blade teetering rotor and the H-34 a four-blade fully articulated rotor; both have constant-chord twisted blades. The NASA model, which is a two-blade teetering system, has constant-chord, nontwisted blades. The disk loadings for these three rotors are approximately as follows: HU-1A, 4.0 psf; H-34, 4.9 psf; NASA model, 2.3 psf.

Blade Motion Analysis

The following measured quantities relating to the blade motions were used in this analysis:

1. Blade root rotation about flapping hinge as function of azimuth.
2. Blade root rotation about pitch axis as function of azimuth.
3. Flapwise bending moments along blade span as function of azimuth.
4. Torsion moments along span as function of azimuth.

Items 1 and 3 were harmonically analyzed.

The blade motions, as used in the present approach for computing the airloads, are classified as either plunging or rotational. The plunging displacements are defined to be the normal displacements of the quarter-chord with respect to the tip-path-plane. The rotational displacements are about the quarter-chord and with respect to the tip-path-plane.

The radial distributions of the plunging displacements at each harmonic of the rotational speed, sine and cosine, are computed by double integration of a Fourier series fit to the radial curvature distributions; the curvature distributions are obtained from the bending stiffness and measured moment distributions at each harmonic (obtained from harmonic analysis of measured moments). The constants of integration are evaluated from the end conditions which include the measured flapwise root rotation at each harmonic. The slopes and plunging velocities of the blades, which are used directly in the airloads computation, are obtained by differentiating the displacement distribution with respect to the radius and time, respectively. The first harmonic flapping, sine and cosine, is obtained by performing an orthogonal analysis of the radial distribution of the first harmonic plunging displacement; the orthogonal functions used are the first five bending mode shapes of the blade. This procedure for computing the blade deflections from the measured moment distributions is, in principle, similar to that reported by Sikorsky (Ref. 38).

For both the HU-1A and the H-34, the only measured data available to determine the pitching rotational motions of the blade sections are the pitch root rotation and the torsional moments at only two radial stations (15 and 50 percent of radius). At each azimuth station, two simultaneous equations are set up and solved for the tip deflection in each of the first two normalized (for unit tip deflection) cantilever torsional modes by making use of their moment distributions and the measured torsional moments at each of the two radii. The rotational deflections are then computed from these tip deflections in each torsion mode, the computed torsional mode shapes, and the pitch root rotations.

In using the above procedures for computing the blade motions from the measured root displacements and the bending and torsion moment distributions, the effects of intermodal coupling on the motions have been neglected; the effects may, however, be important. If the effects of intermodal coupling were to be included, it would be necessary to increase the accuracy of the motion data considerably and perform more extensive calibrations.

It should be noted here, again, that this approach of using the measured motion and strain data to compute the airloads was taken only as an attempt to separate the airloads problem from the over-all aeroelastic problem and, thereby, enable the focusing of effort on the formulation of an adequate aerodynamic representation. Although some known constraints were not satisfied because of this approach, it was successful in that the objective was attained; now that the basic aerodynamic representation has been developed, effort can be spent on refinements and the complete aeroelastic problem.

RESULTS

Measured and computed airloads are presented for the following configurations and flight conditions:

NASA Model; μ = 0.08, 0.15, 0.29

H-34; μ = 0.18, 0.29

HU-1A; μ = 0.21, 0.26

Two of these will be emphasized — the NASA model at μ = 0.15, and the HU-1A at μ = 0.26. For these two cases, the airloads are compared in two ways: (1) azimuthal distributions at each radial station, and (2) radial distributions of the steady and the sine and cosine components of each of the first eleven harmonics. The two forms of presentation are used to emphasize the fact that apparent good agreement with respect to azimuthal distributions does not necessarily guarantee good agreement with respect to particular harmonics. Comparisons should always be made with respect to the spanwise distributions of the harmonics of the airloads because it is believed that this is the form most suitable for the derivation of the forces transmitted to the fuselage and the generalized forces for estimating oscillatory blade stresses.

All graphs of oscillatory airloads for a given rotor and flight condition are presented on the same scale to facilitate inspection of relative amplitudes at the various harmonics and advance ratios. Curves have been passed through

the experimental and theoretical points to indicate the form of the spanwise distribution of airload components. Unfortunately, the points are not always sufficiently dense to define a unique curve.

Mach number and Reynolds number corrections have not been made, although these could be introduced without modifying the calculation procedure developed. A constant lift curve slope of 5.73 per radian was used, except in those calculations in which stall effects were included. Stall effects were included in the calculations made for the HU-1A at μ = 0.26 by limiting the circulatory lift, as previously described.

A typical induced velocity distribution, obtained from one of the computations (NASA model, μ = 0.15, nine radial segments), is presented in Table 1. The rows in the table are the radial distributions from the root to the tip of the induced velocity at each azimuth position from $\psi = 0^\circ$ to $\psi = 360^\circ$, in 15° increments. These are the induced velocities <u>on the blade</u> as it rotates and are, therefore, in the rotating coordinate system.

It is interesting to note that the computed induced velocity distributions are always such as to <u>oppose</u> the retreating blade tip stall which has always been predicted on the basis of an assumed uniform inflow distribution; this is more clearly evident from Table 2 in which the distribution of the ratios of the instantaneous <u>effective</u> angle of attack to an angle of 14° is presented. Also to be noted are the positive induced velocities (up-wash) and their relative position in the disk. Regarding this point, it should be remembered that these

are the induced velocities on the blade for its various positions in the rotor disk; furthermore, the up-wash through the disk which has been observed and photographed by other investigators is the result of the time-averaged induced velocities at fixed points of the disk as the blades rotate (i.e., the steady component of the periodic induced velocities in the nonrotating coordinate system).

NASA Model, $\mu = 0.15$

The wake time history used for these computations was defined by the tunnel speed, tip-path-plane inclination, and an assumed uniform value of induced velocity based on momentum theory. The wake used corresponded to three revolutions of the rotor. The measured collective pitch angle was used. For the computation using five radial control points, the first harmonic flapping was estimated in order to satisfy, approximately, the condition that the first harmonic airload moment about the teetering pin be zero. Only the first harmonic flapping motions were included — the blade elastic deformations, pitching and higher harmonic flapping motions were neglected.

The computed and measured azimuthal airload distributions are presented in Fig. 3. The computed curves are based on five radial control points and, to provide a more direct comparison of the oscillatory components, they are corrected for the difference between the computed and experimental steady airloads. Good over-all agreement is indicated. A much more stringent

comparison is made in Fig. 4 where the radial distributions of the sine and cosine components at each harmonic of the airloads are presented.

Calculated and measured steady airload distributions are shown on Fig. 4a. The computed curve based on five radial control points (in fact, the same radial stations at which the airloads were measured) is shown as a dashed line, and the curve based on nine radial points is shown as a dotted line; a solid line is drawn through the experimental data in these graphs. The form of the steady airload distribution is obtained, but the computed magnitudes are too large.

First harmonic cosine and sine load distributions are shown on Fig. 4b. Attention is again called to the fact that the first harmonic flapping was chosen to yield a cosine airload distribution having a nearly zero moment about the flapping hinge for the computation based on five radial control points. It is immediately evident that the computed curve based on nine radial control points and this same assumed flapping does not satisfy the cosine lift moment constraint; however, the experimental curve drawn does not satisfy this constraint either. In Ref. 2, the experimental load distribution was evidently made to satisfy the lift moment constraint by requiring sizable negative lifts at $r/R = 0.9$ in both sine and cosine components. Neither of the computed cosine components agrees with the measured distribution as drawn. The computed first harmonic sine components of airload obviously do not satisfy the lift moment constraint, and improvement in agreement would be obtained by imposing this condition. The computed first harmonic airloads were found to be quite sensitive to the first harmonic flapping angle.

Second harmonic components of the airloads are shown on Figure 4c. Theory and experiment agree as to distribution and reasonably well with respect to magnitude.

Third harmonic components are shown on Figure 4d. Reasonable agreement was obtained. There is an interesting point here. Although the first uncoupled unsymmetric bending mode frequency of the model is nearly three per rev (Ref. 2), the calculated airload distribution, in which the elastic motions were ignored, agrees reasonably well with the measured values. Whether or not this is the result of compensating errors is not known at this time.

Figures 4e through 4ℓ are graphs of the computed and measured airloads of the fourth through the eleventh harmonic. In nearly all cases the measured and calculated values agree reasonably well. Because only first harmonic blade motions were included, the computed airloads at harmonics beyond the third are entirely due to the induced velocity distribution. The experimental airloads for harmonics beyond the sixth were obtained by harmonic analysis of the azimuthal distributions given in Reference 1; no correction was made for instrumentation response. A previous report related to this rotor (Ref. 3) indicates that the instrumentation correction is trivial at frequencies corresponding to the sixth harmonic, but at the eleventh harmonic the measured amplitudes would be approximately 20% too high.

In summary, the calculated and measured airload distributions for the model rotor showed qualitative agreement. A relatively simple wake time

history was used; blade flexibility was neglected, and only the first harmonic rigid-body flapping motions were used. Furthermore, known constraints implicit in satisfying the flapping equation of motion were not rigorously satisfied.

HU-1A at $\mu = 0.26$

The computed and measured airloads for the HU-1A at $\mu = 0.26$ are presented in Figures 5 and 6. The wake time history used for these computations was defined by the free stream velocity, tip-path-plane inclination, and an assumed uniform induced velocity derived from momentum considerations. A wake corresponding to two rotor revolutions was used. Measured values of blade root rotation and blade strains were used to determine blade positions, shapes, and velocities; however, the effects of intermodal coupling were neglected when determining these motions. The results of two sets of calculations are presented in Fig. 6: the first, in which only the steady deflections and rigid-body first harmonic motions were included; and the second, in which all the rigid and elastic motions were included. For the case in which the higher harmonic motions were included, the motion and strain data traces were inspected and those motions and strains which were represented by trace deflections of less than 0.02 inches were discarded. Stall effects were included in the manner discussed previously. Airloads were computed at eight radial stations, five of which are the stations at which the airloads were measured.

The azimuthal variations of the measured and computed airloads at each radial station are presented in Fig. 5; the computed airloads presented here are from the computation which included all the rigid and elastic motions. Reasonable agreement is obtained.

The steady component of the airloads are shown on Fig. 6a, and it can be seen that the measured and calculated values are in good agreement.

First harmonic airloads are shown on Fig. 6b. Although the distribution of the computed first harmonic sine component agrees quite well with the measured distribution, the distribution of the computed cosine component does not, especially over the inboard position of the blade. Including the elastic motions and the harmonics of flapping above the first had an effect on the computed airloads, but there are no clear grounds for assessing the necessity for including elastic deformations.

Figure 6c is a graph of the second harmonic airloads. The computed cosine component agrees reasonably well with the measured cosine component but the sine component agreement is poor. Again, elastic deformations used had relatively little effect.

Third harmonic airloads are shown on Fig. 6d. Here, there is a temptation to argue that inclusion of the elastic motions and higher harmonics of flapping is significant — especially because there is a natural flapwise bending frequency in the vicinity of the third harmonic and, therefore, the third harmonic bending motions are relatively large. However, this argument cannot be sustained on the basis of the airloads at a single harmonic because the motions at a given harmonic not only contribute directly to the airloads at

that harmonic but, also, contribute directly to the airloads at the harmonic above and below the given harmonic. For example, examine the comparison of the calculated and measured airloads at the fourth harmonic, Fig. 6e (the third harmonic blade motions contribute directly to the fourth harmonic). Here, the neglect of the elastic and higher harmonic flapping motions apparently yields better agreement.

The fifth and higher harmonics are shown on Figs. 6f through 6ℓ. These are presented as a matter of interest in that they are relatively small in amplitude. The significance of the detailed comparison of the calculated and measured results is obscured by the question of measurement accuracy.

HU-1A at μ = 0.21

Measured and calculated harmonic components of the airloads on the HU-1A at μ = 0.21 are shown in Figure 7. Stall effects were judged to be small and were neglected, and only first harmonic rigid-body motions were retained in the computations. The agreement between calculated and measured results is about the same as that observed for the previous case (HU-1A at μ = 0.26).

NASA Model; μ = 0.08 and 0.29

The computed airloads are based on measured collective pitch, shaft, and first harmonic flapping angles. A wake corresponding to five rotor revolutions was retained for the μ = 0.08 case and two revolutions for the μ = 0.29 case. For each case the wake was positioned on the assumption of a uniform inflow velocity derived from momentum considerations.

A comparison of the theoretical and experimental airloads is presented in Figures 8 and 9. In both cases the mean load was overpredicted.

It is evident that the theoretical first harmonic airload distributions do not satisfy the requirement that the moment of the airload about the flapping hinge be zero; but the measured cosine airload at μ = 0.29 does not satisfy this requirement either. Introduction of the rigid-body flapping equation into the airload analysis would force the theoretical distribution to satisfy the airload moment condition but, then, the calculated flapping angles would not agree with the measured values. Resolution of this apparent incompatibility could be obtained if the root rotation (which is an item that was measured) contained an appreciable first harmonic bending slope superimposed on the rigid-body flapping. However, the displacement data presented in Ref. 2 indicates this is unlikely.

Relatively good agreement was obtained for the second harmonic cosine components, but the small sine components are not well predicted. It should be noted here, again, that the first harmonic flapping velocity and cyclic pitch influence the airloads quite strongly.

There is reasonable agreement between calculated and measured values for the third harmonic. For this particular rotor, the third harmonic is appreciably larger at μ = 0.08 than at 0.29.

Agreement between measured and calculated curves is good for the fourth

and fifth harmonic components, but the sixth at μ = 0.08 is underpredicted at the outboard stations.

Comparison of the airloads for the seventh through eleventh harmonics is also presented. It was pointed out previously that these measured components were obtained by a harmonic analysis of the azimuthal distribution of the airloads given graphically in Ref. 1. Because no corrections were made for instrumentation response (and Ref. 3 indicates that the recorded eleventh harmonic would be approximately 20% too large), the comparison should be viewed as qualitative. In addition, many of the experimental points correspond to trace amplitudes less than 10% of the total oscillatory amplitudes, and, therefore, the accuracy of these results is uncertain.

Flight Tests: H-34, μ = 0.18

Only rigid-body first harmonic motions were used in calculating the H-34 airloads at an advance ratio of 0.18. These calculated airloads are compared in Figure 10 with the measured airloads. There is no measured eleventh harmonic, so only the computed distribution is shown for this harmonic. Again, stall effects and Mach number effects were neglected. Agreement between the computed and measured airloads certainly leaves something to be desired, but it is again noted that the first harmonic airload moment is not zero for the computed distribution. The calculated steady load is less than the measured, which is the inverse of the situation found with the wind tunnel model.

Flight Tests: H-34, μ =0.29

For the H-34 at an advance ratio of 0.29, the calculated airloads are compared with measured airloads in Figure 11. Only rigid-body first harmonic motions were included in the computations shown. Again, Mach number and stall effects were neglected.

It was pointed out previously that the experimental data presented here represents only a very small portion of that obtained during the NASA tests. Many conditions other than steady state were investigated during each flight. This obviously required the judicious setting of data channel gains to insure that data were obtained for flight maneuver conditions. Unfortunately, these practical limitations restricted certain of the blade motion and strain trace deflections to relatively small values when steady-state level flight conditions were flown. Superimposed on possible reading inaccuracies are the errors of unknown magnitude that result from conversion of the strain and motion data to deflections and velocities. For these reasons, and because compensating errors might be introduced implicitly through the approximations used in the theory, the calculations were made neglecting the blade elastic motions.

CONCLUDING REMARKS

It is believed that the results obtained to date in this continuing study indicate that accurate calculation of the periodic aerodynamic loads on rotary wings is feasible. Permissible approximations and assumptions are not yet clearly defined. The effect of wake distortion may be important, but a good approximation for the wake displacement time histories should be found and used before a conclusion is reached. Even the number of spanwise stations required for computation purposes may be a function of flight condition due to the rapid loading changes encountered when sections of the blades stall or Mach number effects become important.

Treatment of the combined performance, aerodynamic loads, and blade response problems is believed to be necessary. However, the possibility of considering the blades to be rigid for purposes of calculating the forcing functions and then deriving the elastic response and, subsequently, superimposing corresponding damping loads cannot be rejected.

The above discussion is intended only to indicate that the results obtained are encouraging even when the predicted and measured airloads are compared on a most stringent basis. In some cases a small phase shift would produce a redistribution of the sine and cosine components to give better agreement. In addition, the calculated values have borne the burden of any errors in blade position measurement, strain measurement, and the blade physical properties. Wind tunnel corrections were not applied to the model

data and, of course, any departure from steady-state conditions in the experiments were not accounted for in the computations.

Continuing effort on this program should include work on the following:

1) The noncirculatory and separated-flow forces.
2) An improved approximation to the wake displacement time history (distortions) and the effects of the wake in the immediate vicinity of the blade.
3) The satisfaction of the chordwise boundary conditions.
4) The computation of the flapping motions in addition to the airloads.

The noncirculatory forces which are always present when the flow field is unsteady and the separated-flow forces which arise when an airfoil section stalls can be quite appreciable and should be included in any method of predicting the airloads on a rotating wing. In connection with the stall phenomenon and the reversed flow, there are the attendant problems of wake position, its point or area of attachment, and its nature (i.e., the amount and orientation of vorticity contained).

The induced velocities are now computed at the blades and thus are in the rotating coordinate system. For an improved definition of the wake displacement time history, it is necessary to have the periodic induced velocity distribution in the nonrotating coordinate system on or just under the rotor disk. It is possible, with some modifications to the present method, to compute such a velocity distribution.

The attached wake, because of its proximity to the blade, can have a significant effect on the airloads. Thus, a more accurate representation of this portion of the wake is desirable. This could be accomplished by replacing the trailing and shed vortex segments representing the most recent section of the attached wake (i.e., the section corresponding to the last azimuth step) by a distribution more representative of a continuous wake.

The present method is capable of satisfying linear chordwise boundary conditions, but there is some question as to the importance of accounting for a more general chordwise boundary condition when computing the airloads on a rotating wing. This may be important and should be investigated further.

In its present form the method developed for computing the airload distribution requires that the blade motion be specified. However, when the measured motions are used for a given rotor and flight condition, known constraints are not necessarily satisfied. For this reason and the fact that in practical applications (i.e., preliminary rotor design) the motions are not known, it will be necessary to compute the blade motions simultaneously with the airload distributions. It is suggested that this capability be incorporated first for the flapping motion only and subsequently for the remaining motions.

REFERENCES

1. Rabbott, J. P., Jr. and Churchill, G. B. Experimental Investigation of the Aerodynamic Loading on a Helicopter Rotor Blade in Forward Flight NACA RM L56107 25 October 1956

2. Mayo, A. P. Comparison of Measured Flapwise Structural Bending Moments on a Teetering Rotor Blade with Results Calculated from the Measured Pressure Distribution NASA Memo 2-28-59L March 1959

3. Rabbott, J. P., Jr. Static-Thrust Measurements of the Aerodynamic Loading on a Helicopter Rotor Blade NACA TN 3688 July 1956

4. Martin, George B. Helicopter Main Rotor Blades Cornell Aeronautical Laboratory Report No. BB-427-S-1 May 2, 1946

5. Hirsch, H., Kline, J. and Mertens, R. A Preliminary Design Study of Main Rotor Blades for a Variable Stiffness Flight Test Program Cornell Aeronautical Laboratory Report No. BB-427-S-2 September 16, 1946

6. Kline, J. Structural Analysis of Fiberglas Main Rotor Blade for the R-5 Helicopter Cornell Aeronautical Laboratory Report No. BB-427-S-3 February 18, 1947

7. Hirsch, H. and Mertins, J. Fabrication Procedure for Fiberglas Main Rotor Blades for the R-5 Helicopter Cornell Aeronautical Laboratory Report No. BB-427-S-4 January 17, 1947

8. Weichsel, H., Jr. R-5 Helicopter Variable Stiffness Blade Program Instrumentation and Shakedown Flight Proposal Cornell Aeronautical Laboratory Report No. BB-427-S-5 September 18, 1947

9. Carpenter, J. E. and Mertens, J. R. Structural Test of a Main Rotor Blade for the R-5 Helicopter, Blade Stiffness #2 Cornell Aeronautical Laboratory Report No. BB-427-S-6 January 23, 1948

10. Hirsch, H., Guske, E. and Weichsel, H., Jr. (Edited by Kidd, E.A.) H-5 Variable Stiffness Blade Program, Instrumentation and Shakedown Flight Phase Cornell Aeronautical Laboratory Summary Report No. BB-427-S-9 April 15, 1951

11. Hirsch, H. and Kline, J. H-5 Variable Stiffness Blade Program-- An Experimental Investigation Part I - Harmonic Reduction of Measured Blade Beam Bending Moment Data Cornell Aeronautical Laboratory Report No. BB-427-S (AF Technical Report No. 6329, Part I) December 1951

12. Hirsch, H. and Kline, J. H-5 Variable Stiffness Blade Program - An Experimental Investigation Part II - Blade Beam Beanding Moment Envelopes Cornell Aeronautical Laboratory Report No. BB-427-S (AF Technical Report No. 6329, Part 2) January 1952

13. Hirsch, H. and Kline, J. H-5 Variable Stiffness Blade Program - An Experimental Investigation Part III - Evaluation of Rotor Blade Resonant Bending Effects Cornell Aeronautical Laboratory Report No. BB-427-S (AF Technical Report No. 6329, Part 3) January 1952

14. Kline, J. H-5 Variable Stiffness Blade Program - An Experimental Investigation Part IV - Harmonic Reduction of Measured Blade Motion and Control Force Data Cornell Aeronautical Laboratory Report No. BB-427-S AF Technical Report No. 6329, Part 4 April 1952

15. Kline, J. H-5 Variable Stiffness Blade Program - An Experimental Investigation Part V - Evaluation of Blade Beam Bending Data Measured by Three Helicopter Manufacturers Cornell Aeronautical Laboratory Report No. BB-427-S AF Technical Report No. 6329, Part 5 June 1952

16. Daughaday, H. and Kline, J. H-5 Variable Stiffness Blade Program - An Experimental Investigation Part VI - A Tentative Empirical Criterion for the Design of Rotor Blades for Higher Mode Resonances Cornell Aeronautical Laboratory Report No. BB-427-S AF Technical Report No. 6329, Part 6 November 1952

17. Weichsel, H., Jr. Helicopter Flight Test Technique, Variable Blade Stiffness Program Presented at the 5th Annual Forum of the American Helicopter Society on May 12 and 13, 1949

18. Flax, A. H. and Goland, L. Dynamic Effects in Rotor Blade Bending Cornell Aeronautical Laboratory Report BB-427-S-10 Journal of Aeronautical Sciences Vol. 18, No. 12 December 1951

19. Hirsch, H. The Contribution of Higher Mode Resonance to Helicopter Rotor Blade Bending Presented at IAS Meeting January 1952

20. Daughaday, H. and Kline, J. An Approach to the Determination of Higher Harmonic Rotor Blade Stresses Cornell Aeronautical Laboratory Report No. CAL-52 Proc. Ninth Annual Forum, American Helicopter Society, Inc. May 1953

21. Weichsel, H., Jr. YR-6A Helicopter Vibration Absorber and Vibration Isolator - Flight Test Survey Cornell Aeronautical Laboratory Report No. SB-429-F-1 August 1947

22. Kidd, E. A. Vibration Measurements of a Sikorsky H-5 Fuselage with CAL Fiberglas Blades Cornell Aeronautical Laboratory Report No. BB-427-S-11 February 9, 1951

23. Mangler, K. W. Calculation of the Induced Velocity Field of a Rotor RAE Report No. Aero. 2247 February 1948

24. DuWaldt, F. A. and Gates, C. An Experimental and Theoretical Study of the Low Frequency Flapping-Pitching Flutter of a Hovering Rotor Blade Cornell Aeronautical Laboratory Report No. SB-680-S-2 September 1952

25. Chang, T. T. A Flutter Theory for a Flexible Helicopter Rotor Blade in Vertical Flight Cornell Aeronautical Laboratory Report No. SB-862-S-1 July 1954

26. Daughaday, H. and Kline, J. An Investigation of the Effect of Virtual Delta-Three Angle and Blade Flexibility on Rotor Blade Flutter Cornell Aeronautical Report No. SB-862-S-2 August 1954

27. Daughaday, H. and DuWaldt, F. The Effect of Blade Root Properties on the Natural Mode Shapes, Bending Moments and Shears of a Model Helicopter Rotor Blade Cornell Aeronautical Laboratory Report No. SB-862-S-3 September 1955

28. Daughaday, H., DuWaldt, F. and Gates C. Investigation of Helicopter Rotor Flutter and Load Amplification Problems Cornell Aeronautical Laboratory Report No. SB-862-S-4 August 1956

29. Loewy, R. G. A Two-Dimensional Approximation to the Unsteady Aerodynamics of Rotary Wings Cornell Aeronautical Laboratory Report No. 75 IAS Preprint No. 605 October 1955

30. Daughaday, H. and DuWaldt, F. The Effect of Blade Root Properties on the Natural Mode Shapes, Bending Moments and Shears of a Model Helicopter Rotor Blade Journal of the American Helicopter Society Vol. 1, No. 2 April 1956

31. Daughaday, H., DuWaldt, F. and Gates, C. Investigation of Helicopter Blade Flutter and Load Amplification Problems IAS Preprint No. 705 January 31, 1957 and Journal of the American Helicopter Society Vol. 2, No. 3 July 1957

32. DuWaldt, F. A., Gates, C. A. and Piziali, R. A. Investigation of Helicopter Rotor Blade Flutter and Flapwise Bending Response in Hovering WADC Technical Report No. 59-403 August 1959

33. DuWaldt, F. A. and Piziali, R. A. Comparison of Theoretical and Experimental Flutter Results for a Full-Scale Helicopter Rotor WADD Technical Report No. 60-692 July 1960

34. DuWaldt, F. A., Gates, C. A. and Piziali, R. A. Investigation of the Flutter of a Model Helicopter Rotor Blade in Forward Flight WADD Technical Report No. 60-328 July 1960

35. DuWaldt, F. A. and Gates, C. A. Experimental and Theoretical Investigation of the Flutter Characteristics of a Model Helicopter Rotor Blade in Forward Flight Cornell Aeronautical Laboratory Report No. BB-1504-S-1 ASD Technical Report 67-712 February 1962

36. Burpo, F. Measurement of Dynamic Airloads on a Full Scale Semi-Rigid Rotor Bell Helicopter Corporation Report No. 525-099-001 TRECOM Technical Report 62-42 June 1962

37. (no author) Information and Preliminary Data on H-34 Helicopter Rotor Blade Dynamic Airloads and Motions Measured in Flight NASA May 1961

38. Caseria, R. and Marlatt, W. Conversion of Blade Bending Moment Measurements to Blade Deflections Sikorsky Helicopter Corporation Report No. SER-50053 October 24, 1958

Table I

COMPUTED INDUCED VELOCITY DISTRIBUTION ON BLADE AS A FUNCTION OF AZIMUTH POSITION; NASA MODEL; $\mu = 0.15$

	r/R = 0.31	0.45	0.55	0.65	0.75	0.85	0.915	0.95	0.985
$\psi = 0°$	-0.3900E 01	-0.4738E 01	-0.4453E 01	-0.6288E 01	-0.1210E 02	-0.1720E 02	-0.2375E 02	-0.2904E 02	-0.3792E 02
	-0.4683E 01	-0.4601E 01	-0.6096E 01	-0.1064E 02	-0.1365E 02	-0.1973E 02	-0.2548E 02	-0.3018E 02	-0.3807E 02
	-0.4193E 01	-0.8256E 01	-0.1115E 02	-0.1286E 02	-0.1688E 02	-0.2196E 02	-0.2685E 02	-0.3090E 02	-0.3776E 02
	-0.7669E 01	-0.9477E 01	-0.1144E 02	-0.1396E 02	-0.1744E 02	-0.2226E 02	-0.2655E 02	-0.3009E 02	-0.3628E 02
	-0.7919E 01	-0.1020E 02	-0.1206E 02	-0.1481E 02	-0.1803E 02	-0.2218E 02	-0.2650E 02	-0.2997E 02	-0.3531E 02
	-0.7186E 01	-0.1005E 02	-0.1228E 02	-0.1597E 02	-0.1965E 02	-0.2274E 02	-0.2487E 02	-0.2641E 02	-0.3031E 02
$\psi = 90°$	-0.7610E 01	-0.1070E 02	-0.1353E 02	-0.1463E 02	-0.1605E 02	-0.1578E 02	-0.1448E 02	-0.1591E 02	-0.2289E 02
	-0.8312E 01	-0.1079E 02	-0.1130E 02	-0.1232E 02	-0.1066E 02	-0.5661E 01	-0.1026E 02	-0.1461E 02	-0.2225E 02
	-0.8530E 01	-0.9337E 01	-0.1012E 02	-0.8719E 01	-0.2393E 01	-0.5622E 01	-0.1099E 02	-0.1534E 02	-0.2259E 02
	-0.7346E 01	-0.8804E 01	-0.8536E 01	-0.2658E 01	-0.2078E 01	-0.6743E 01	-0.1207E 02	-0.1630E 02	-0.2335E 02
	-0.7041E 01	-0.8253E 01	-0.5210E 01	0.1908E-00	-0.2880E 01	-0.7749E 01	-0.1318E 02	-0.1743E 02	-0.2452E 02
	-0.6541E 01	-0.6437E 01	-0.5754E 00	0.1051E-00	-0.3652E 01	-0.8674E 01	-0.1434E 02	-0.1872E 02	-0.2603E 02
$\psi = 180°$	-0.6097E 01	-0.4977E 01	0.1054E 01	-0.2433E-00	-0.4249E 01	-0.9507E 01	-0.1549E 02	-0.2006E 02	-0.2772E 02
	-0.5411E 01	-0.3426E 01	0.1926E 01	-0.3283E-00	-0.4601E 01	-0.1018E 02	-0.1652E 02	-0.2137E 02	-0.2942E 02
	-0.4550E 01	-0.3409E 01	0.1420E 01	-0.2350E-00	-0.4694E 01	-0.1062E 02	-0.1732E 02	-0.2246E 02	-0.3097E 02
	-0.4020E 01	-0.4077E 01	0.9369E-01	0.5399E-01	-0.4426E 01	-0.1072E 02	-0.1777E 02	-0.2320E 02	-0.3222E 02
	-0.3578E 01	-0.5535E 01	-0.4124E 01	-0.7737E 00	-0.3856E 01	-0.1036E 02	-0.1774E 02	-0.2349E 02	-0.3306E 02
	-0.3320E 01	-0.6989E 01	-0.8189E 01	-0.6518E 01	-0.4572E 01	-0.9587E 01	-0.1713E 02	-0.2318E 02	-0.3337E 02
$\psi = 270°$	-0.3353E 01	-0.7845E 01	-0.1067E 02	-0.1319E 02	-0.1318E 02	-0.1203E 02	-0.1753E 02	-0.2279E 02	-0.3328E 02
	-0.3636E 01	-0.8320E 01	-0.1162E 02	-0.1529E 02	-0.1960E 02	-0.2401E 02	-0.2731E 02	-0.3011E 02	-0.3737E 02
	-0.4000E 01	-0.8127E 01	-0.1076E 02	-0.1386E 02	-0.1815E 02	-0.2358E 02	-0.2995E 02	-0.3487E 02	-0.4257E 02
	-0.4345E 01	-0.7633E 01	-0.9319E 01	-0.1202E 02	-0.1609E 02	-0.2211E 02	-0.2832E 02	-0.3329E 02	-0.4162E 02
	-0.4501E 01	-0.6688E 01	-0.7319E 01	-0.8970E 01	-0.1248E 02	-0.1888E 02	-0.2558E 02	-0.3101E 02	-0.3999E 02
	-0.4297E 01	-0.5721E 01	-0.5585E 01	-0.6422E 01	-0.1006E 02	-0.1575E 02	-0.2276E 02	-0.2851E 02	-0.3605E 02

NOTE: THE LETTER E PRECEEDS THE POWER OF TEN ASSOCIATED WITH THE PLACEMENT OF THE DECIMAL POINT. FOR EXAMPLE:

$(\pm)$ 0.yyyy E 02 $\equiv$ $(\pm)$ 0.yyyy X 10^2 = $(\pm)$ yy.yy

$(\pm)$ 0.yyyy E-01 $\equiv$ $(\pm)$ 0.yyyy X 10^{-1} = $(\pm)$ 0.0yyyy

Table 2

COMPUTED NONDIMENSIONAL EFFECTIVE ANGLE OF ATTACK DISTRIBUTION ALONG BLADE AS A FUNCTION OF AZIMUTH POSITION (NONDIMENSIONALIZED TO 14 DEGREES); NASA MODEL; $\mu = 0.15$

	r/R = 0.31	0.45	0.55	0.65	0.75	0.85	0.915	0.95	0.985
$\psi = 0°$	0.4925E-01	0.5495E-01	0.5923E-01	0.5816E-01	0.5082E-01	0.4624E-01	0.3941E-01	0.3384E-01	0.2414E-01
	0.4408E-01	0.5162E-01	0.5156E-01	0.4603E-01	0.4431E-01	0.3871E-01	0.3336E-01	0.2877E-01	0.2064E-01
	0.4248E-01	0.3868E-01	0.3702E-01	0.3784E-01	0.3501E-01	0.3136E-01	0.2740E-01	0.2376E-01	0.1709E-01
	0.2823E-01	0.3186E-01	0.3223E-01	0.3160E-01	0.2972E-01	0.2651E-01	0.2336E-01	0.2037E-01	0.1459E-01
	0.2409E-01	0.2632E-01	0.2693E-01	0.2598E-01	0.2458E-01	0.2230E-01	0.1913E-01	0.1627E-01	0.1151E-01
	0.2274E-01	0.2300E-01	0.2281E-01	0.2039E-01	0.1852E-01	0.1776E-01	0.1720E-01	0.1649E-01	0.1323E-01
$\psi = 90°$	0.1866E-01	0.1865E-01	0.1756E-01	0.1941E-01	0.2041E-01	0.2330E-01	0.2619E-01	0.2521E-01	0.1825E-01
	0.1450E-01	0.1630E-01	0.1938E-01	0.2089E-01	0.2577E-01	0.3383E-01	0.2908E-01	0.2464E-01	0.1688E-01
	0.1237E-01	0.1817E-01	0.2046E-01	0.2565E-01	0.3657E-01	0.3321E-01	0.2749E-01	0.2303E-01	0.1563E-01
	0.1505E-01	0.1921E-01	0.2357E-01	0.3595E-01	0.3778E-01	0.3245E-01	0.2675E-01	0.2239E-01	0.1510E-01
	0.1601E-01	0.2136E-01	0.3146E-01	0.4279E-01	0.3867E-01	0.3304E-01	0.2716E-01	0.2270E-01	0.1522E-01
	0.1817E-01	0.2766E-01	0.4384E-01	0.4601E-01	0.4067E-01	0.3478E-01	0.2850E-01	0.2378E-01	0.1587E-01
$\psi = 180°$	0.2048E-01	0.3429E-01	0.5162E-01	0.4966E-01	0.4376E-01	0.3743E-01	0.3059E-01	0.2550E-01	0.1696E-01
	0.2393E-01	0.4226E-01	0.5873E-01	0.5441E-01	0.4780E-01	0.4083E-01	0.3331E-01	0.2776E-01	0.1843E-01
	0.2846E-01	0.4617E-01	0.6288E-01	0.5983E-01	0.5254E-01	0.4480E-01	0.3655E-01	0.3046E-01	0.2024E-01
	0.3151E-01	0.4751E-01	0.6450E-01	0.6567E-01	0.5794E-01	0.4928E-01	0.4027E-01	0.3360E-01	0.2240E-01
	0.3437E-01	0.4520E-01	0.5679E-01	0.6853E-01	0.6366E-01	0.5425E-01	0.4446E-01	0.3716E-01	0.2491E-01
	0.3680E-01	0.4208E-01	0.4796E-01	0.5854E-01	0.6618E-01	0.5945E-01	0.4912E-01	0.4121E-01	0.2785E-01
$\psi = 270°$	0.3838E-01	0.4113E-01	0.4310E-01	0.4504E-01	0.5155E-01	0.5821E-01	0.5183E-01	0.4479E-01	0.3090E-01
	0.3961E-01	0.4186E-01	0.4265E-01	0.4223E-01	0.4064E-01	0.3932E-01	0.3796E-01	0.3574E-01	0.2714E-01
	0.4147E-01	0.4518E-01	0.4726E-01	0.4740E-01	0.4513E-01	0.4154E-01	0.3523E-01	0.2996E-01	0.2116E-01
	0.4368E-01	0.4887E-01	0.5241E-01	0.5235E-01	0.4967E-01	0.4447E-01	0.3828E-01	0.3295E-01	0.2332E-01
	0.4604E-01	0.5267E-01	0.5744E-01	0.5836E-01	0.5559E-01	0.4894E-01	0.4172E-01	0.3569E-01	0.2531E-01
	0.4833E-01	0.5468E-01	0.5987E-01	0.6140E-01	0.5761E-01	0.5165E-01	0.4382E-01	0.3738E-01	0.2647E-01

NOTE: THE LETTER E PRECEEDS THE POWER OF TEN ASSOCIATED WITH THE PLACEMENT OF THE DECIMAL POINT. FOR EXAMPLE:

$$(\pm)\ 0.yyyy\ E\ 02 \equiv (\pm)\ 0.yyyy \times 10^{2} = (\pm)\ yy.yy$$

$$(\pm)\ 0.yyyy\ E\text{-}01 \equiv (\pm)\ 0.yyyy \times 10^{-1} = (\pm)\ 0.0yyyy$$

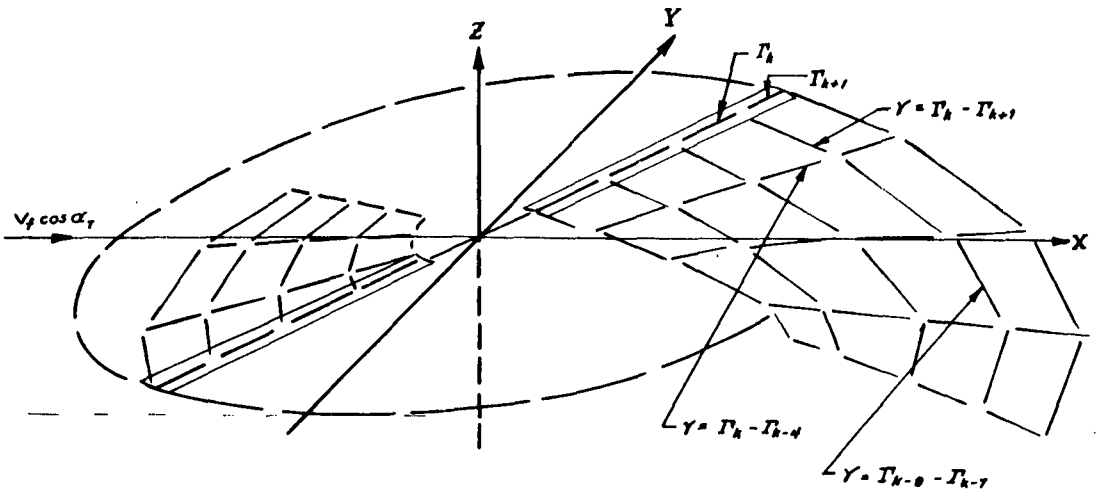

Figure 1. PICTORIAL EXAMPLE OF THE INITIAL PORTION OF THE WAKE OF A TWO-BLADE ROTOR DIVIDED INTO FOUR (i.e. n = 4) RADIAL SEGMENTS

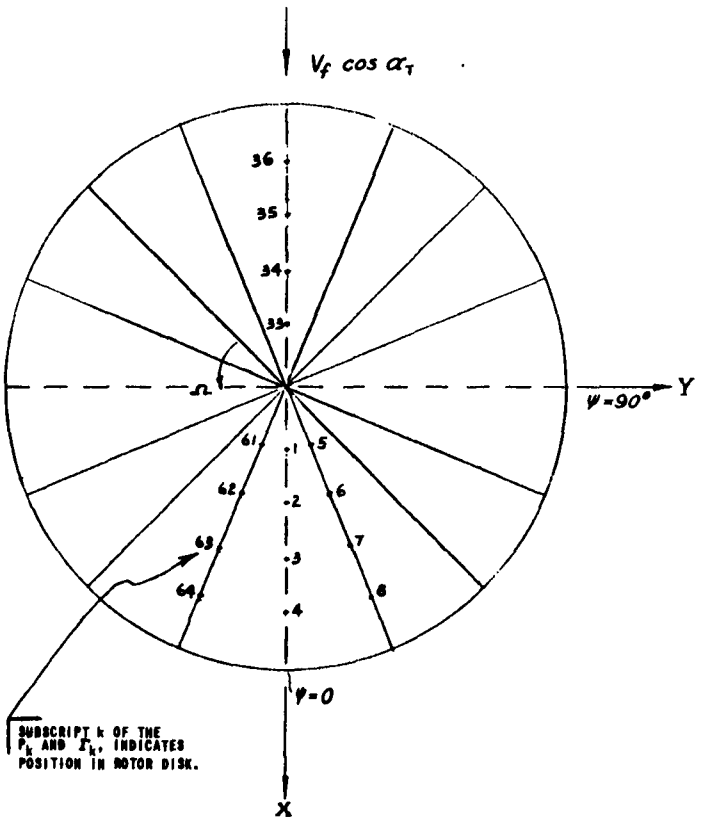

Figure 2. SAMPLE MAP OF COMPUTATION CONTROL POINTS IN TIP PATH PLANE FOR n = 4, N = 16

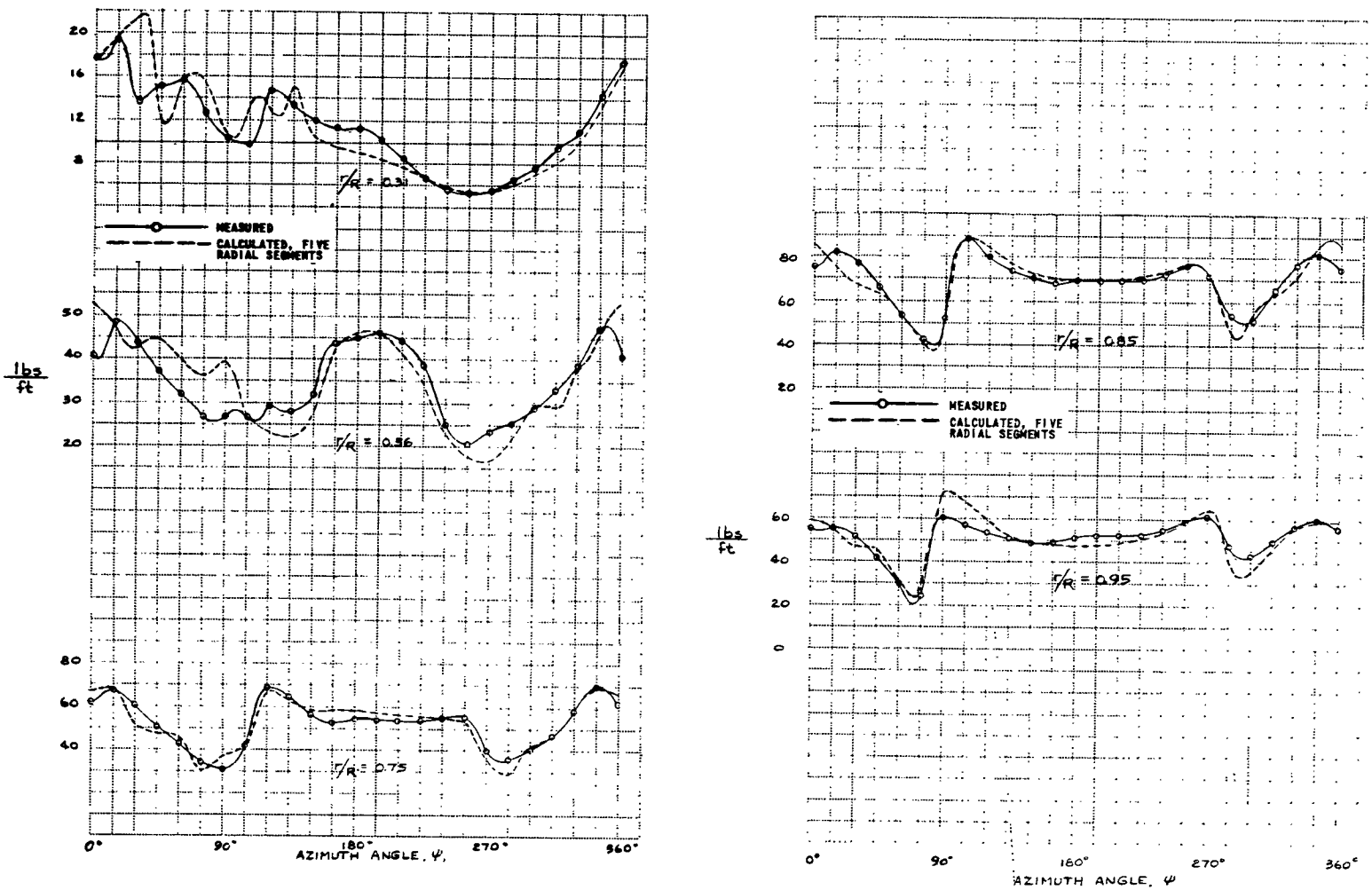

Figure 3. AZIMUTHAL VARIATION OF AIRLOADS FOR NASA MODEL ROTOR; $\mu = 0.15$

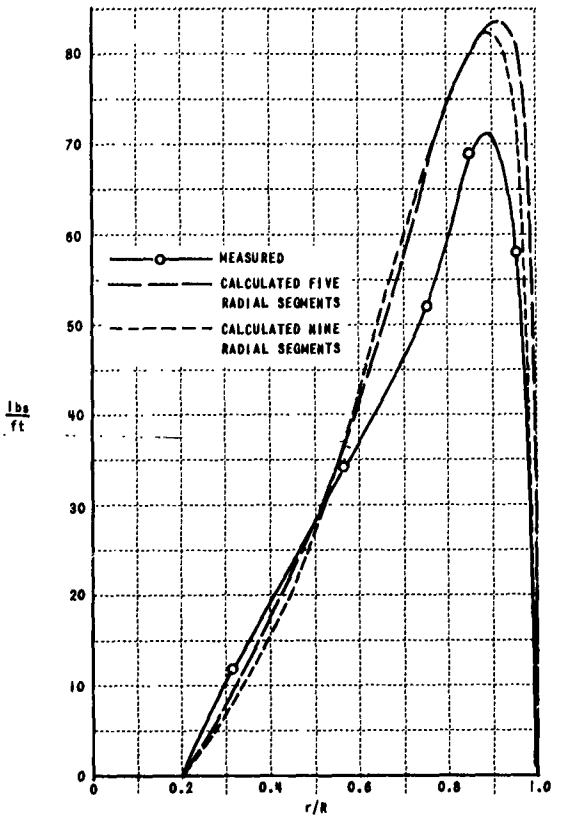

Figure 4. SPANWISE DISTRIBUTIONS OF THE HARMONICS OF THE MEASURED AND COMPUTED AIRLOADS (a). ZEROTH HARMONIC (STEADY) AIRLOADS; NASA MODEL; μ = 0.15

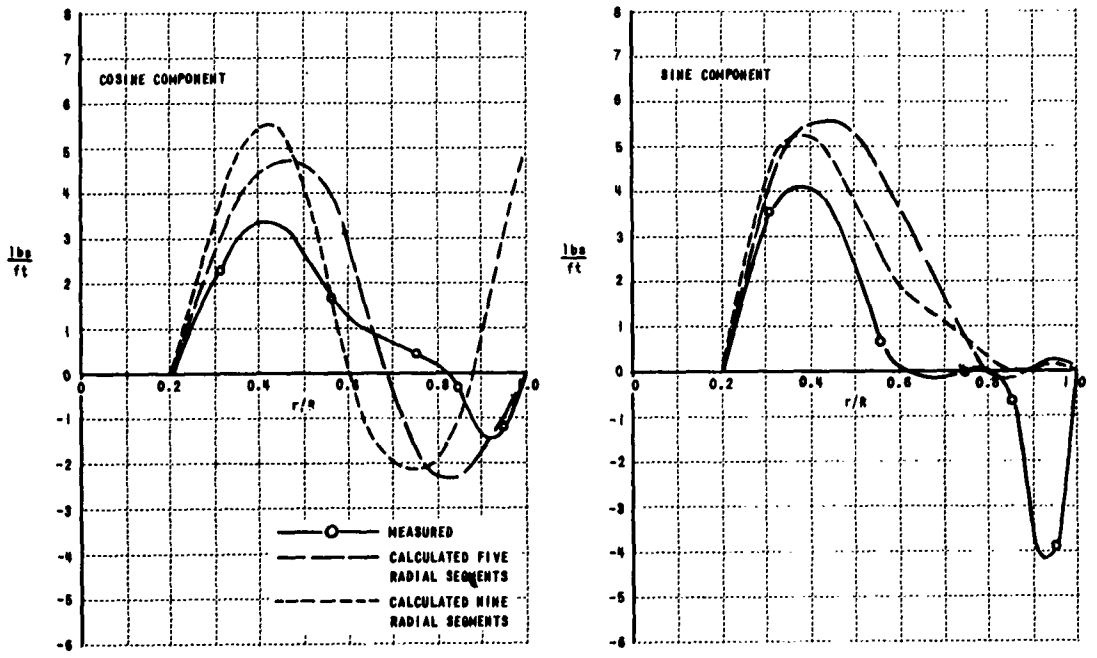

Figure 4b. 1st HARMONIC AIRLOADS; NASA MODEL; μ = 0.15

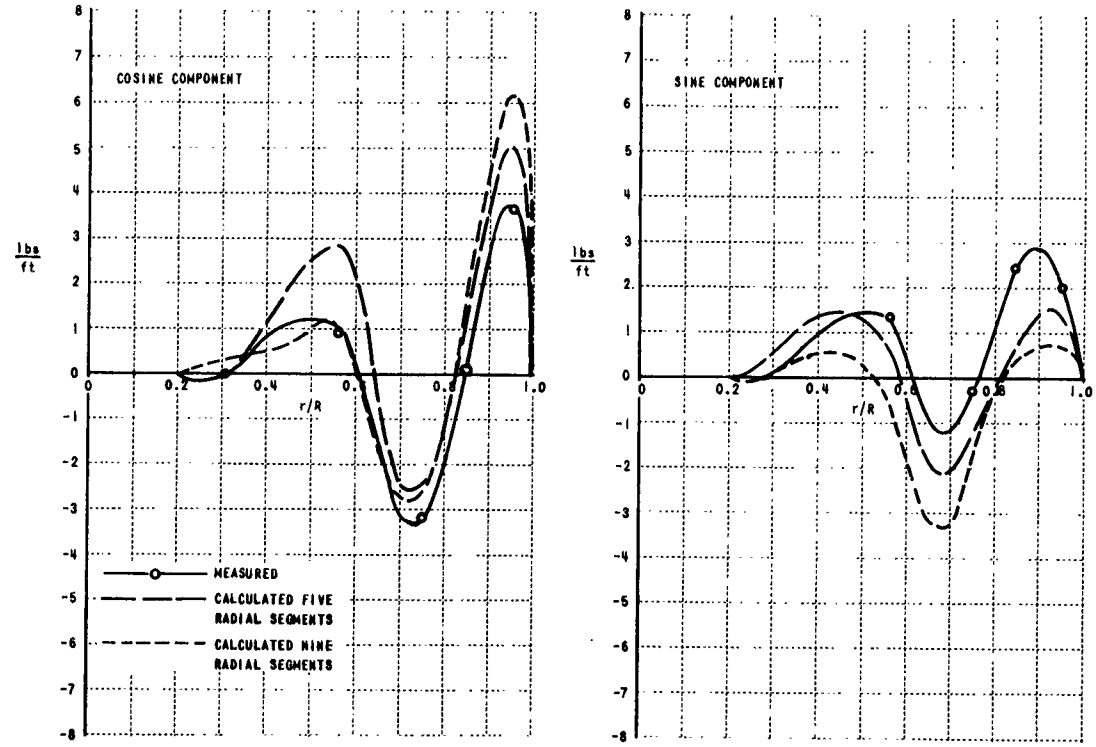

Figure 4e. 4th HARMONIC AIRLOADS; NASA MODEL; $\mu = 0.15$

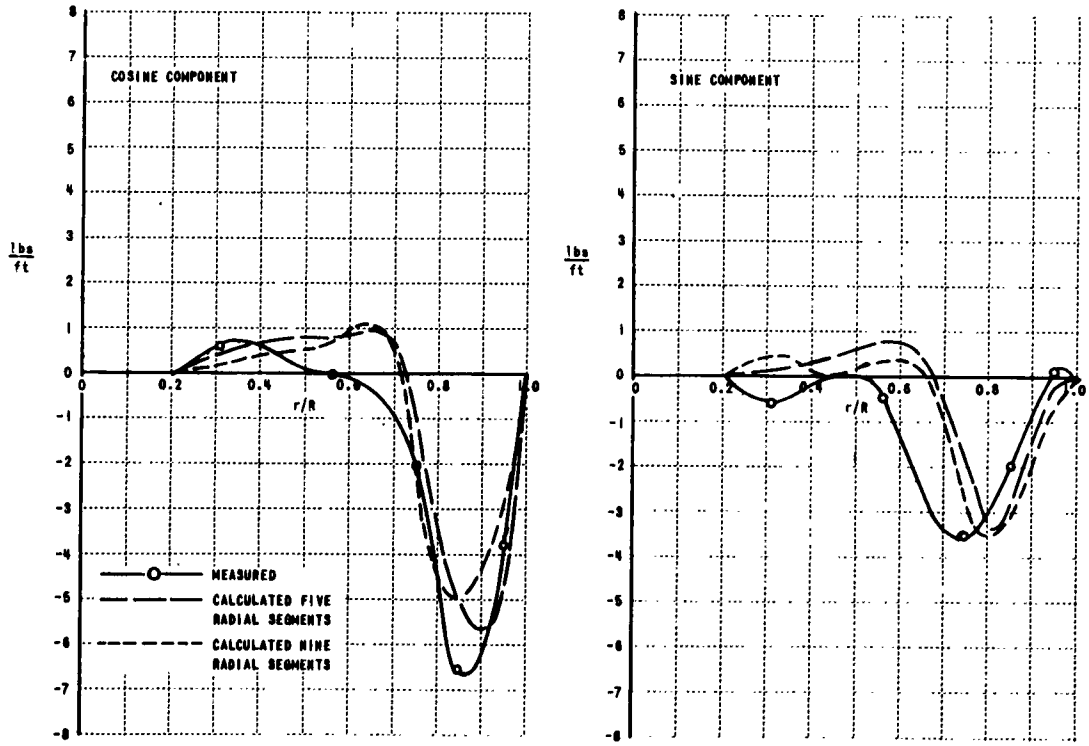

Figure 4f. 5th HARMONIC AIRLOADS; NASA MODEL; $\mu = 0.15$

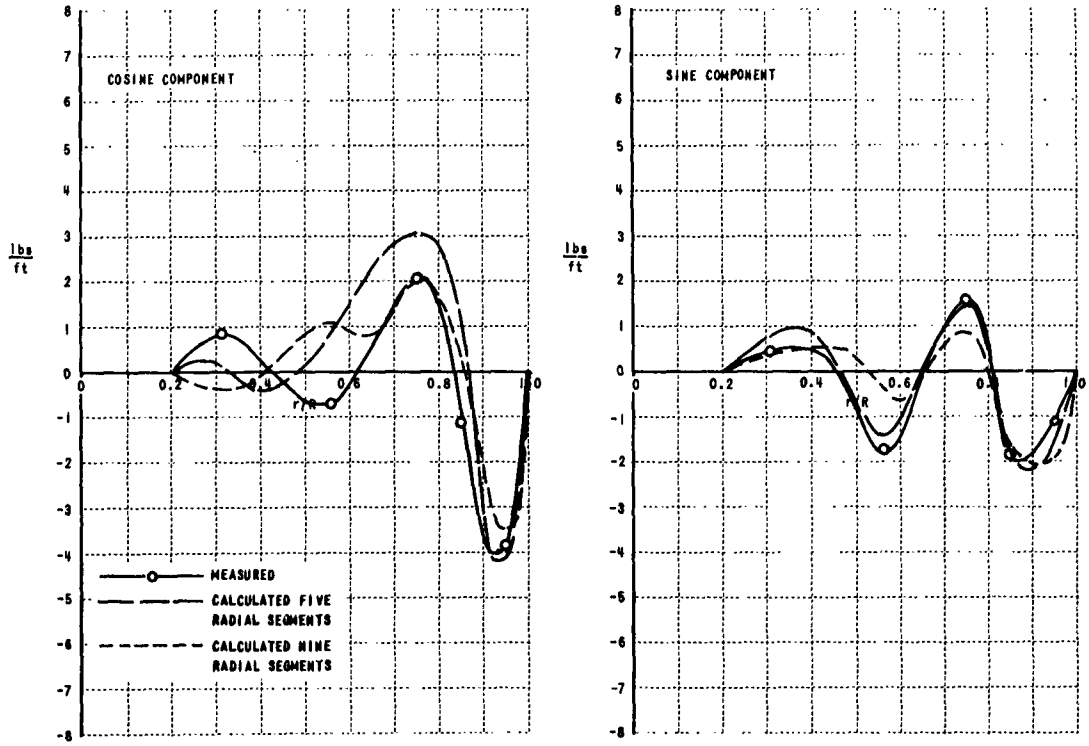

Figure 4g. 6th HARMONIC AIRLOADS; NASA MODEL; μ = 0.15

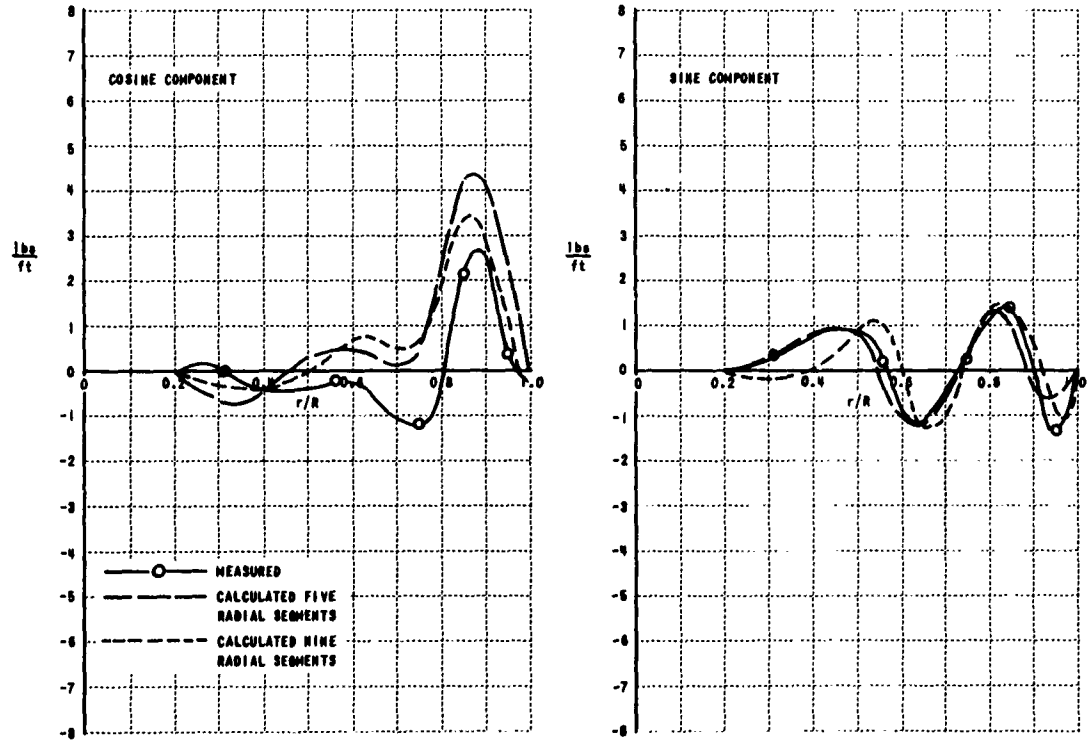

Figure 4h. 7th HARMONIC AIRLOADS; NASA MODEL; μ = 0.15

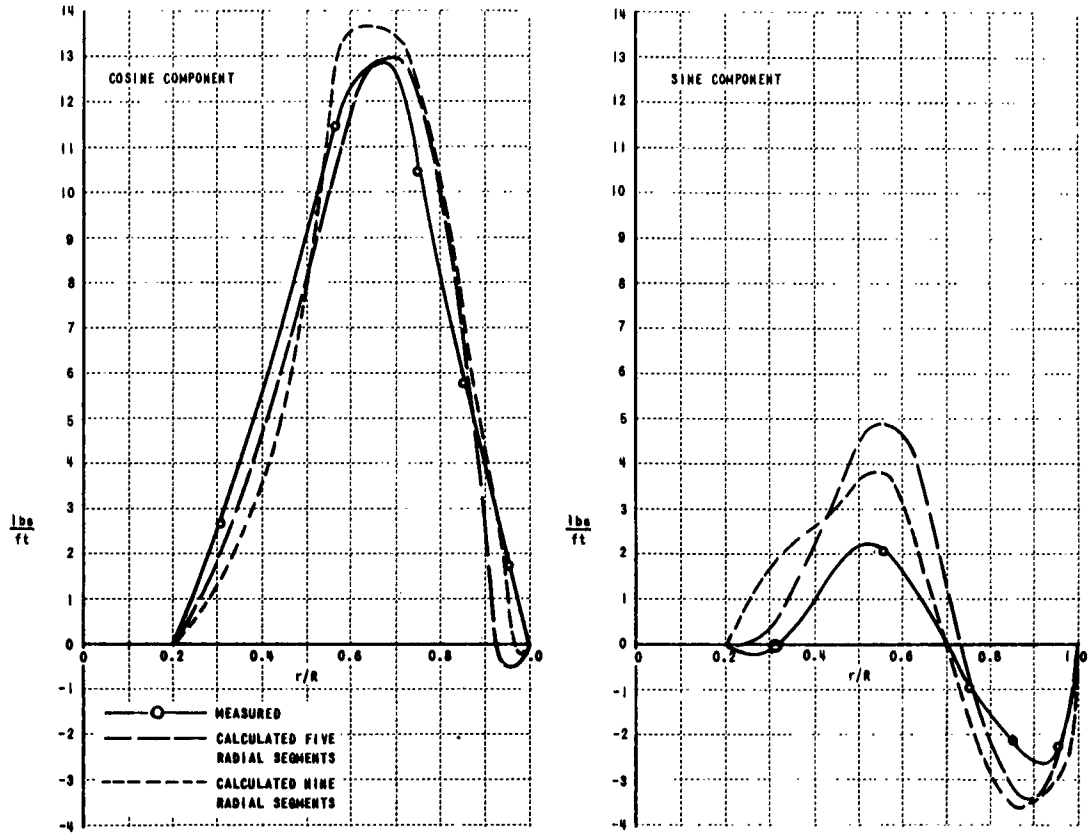

Figure 4c. 2nd HARMONIC AIRLOADS; NASA MODEL; $\mu = 0.15$

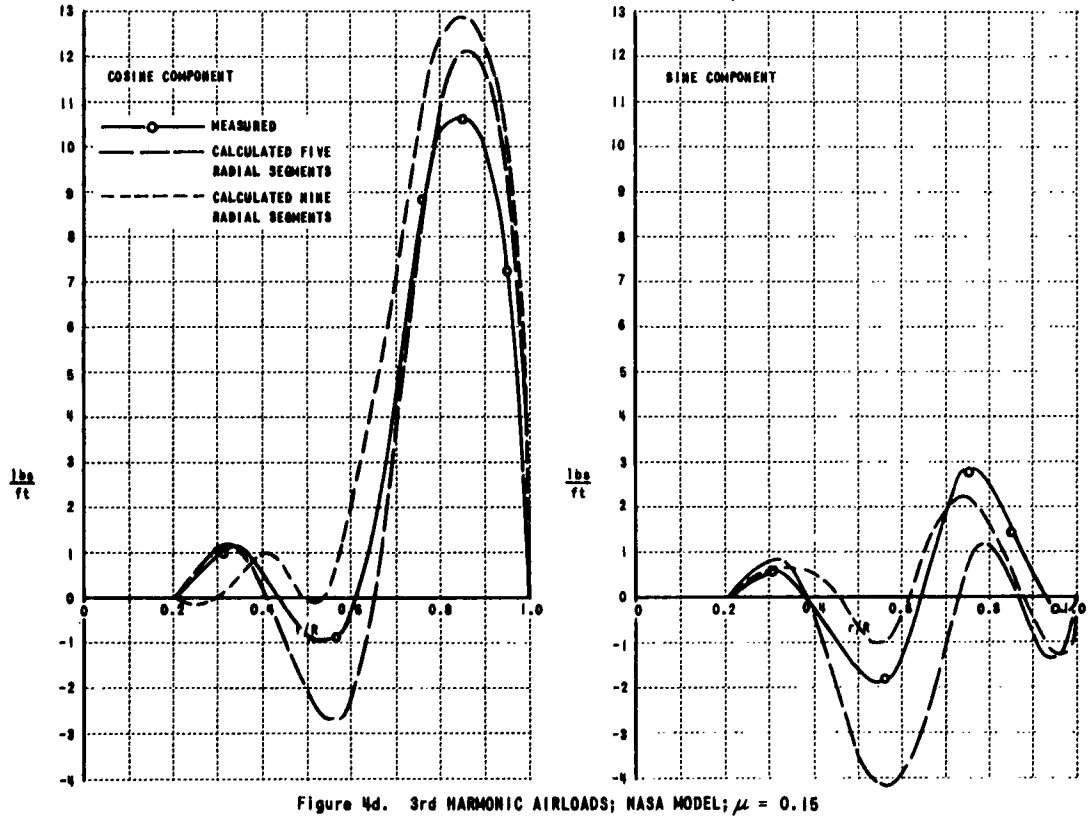

Figure 4d. 3rd HARMONIC AIRLOADS; NASA MODEL; $\mu = 0.15$

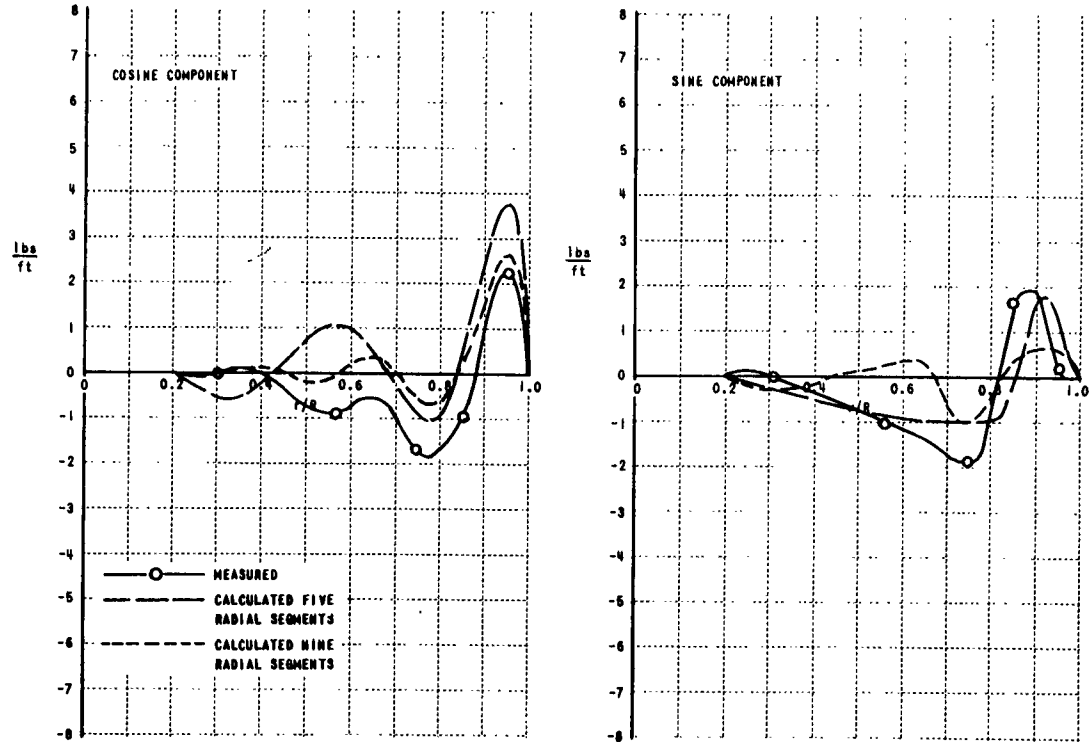

Figure 4i. 8th HARMONIC AIRLOADS; NASA MODEL; $\mu = 0.15$

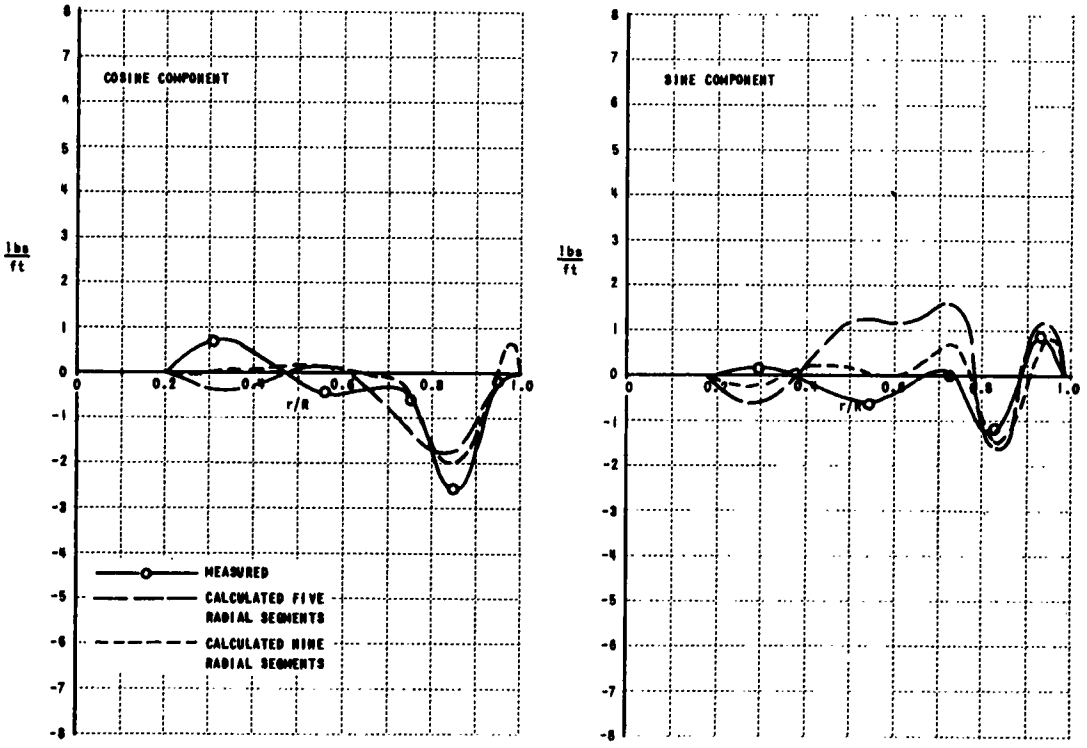

Figure 4j. 9th HARMONIC AIRLOADS; NASA MODEL; $\mu = 0.15$

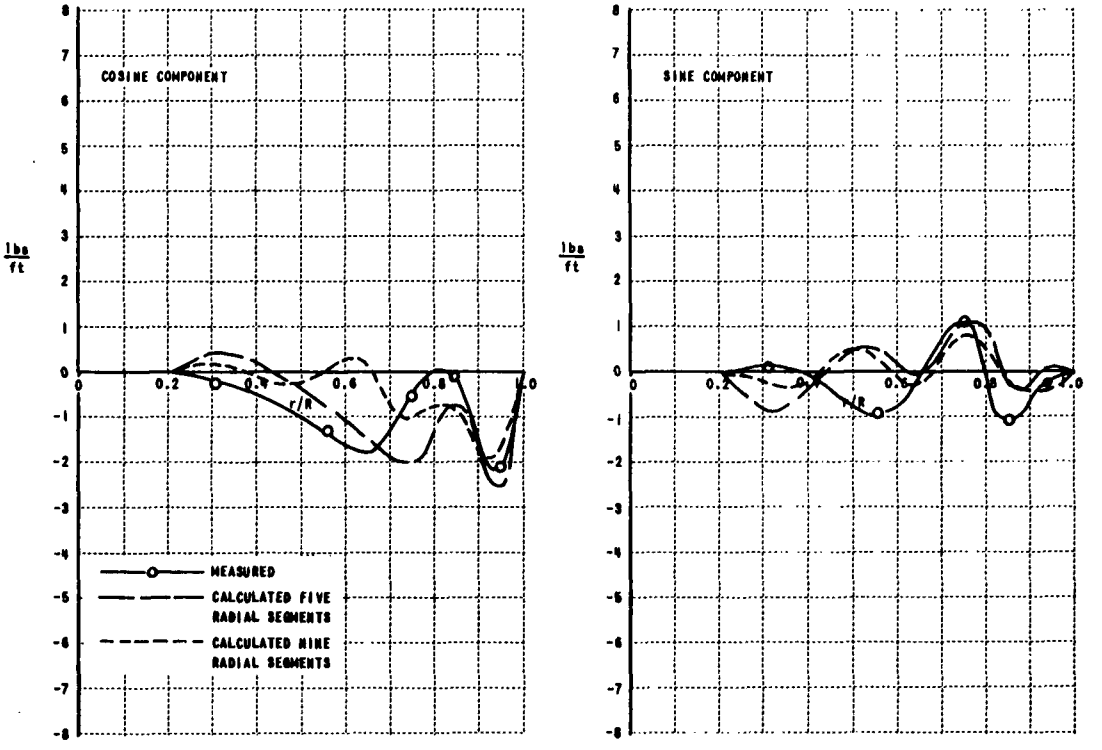

Figure 4k. 10th HARMONIC AIRLOADS; NASA MODEL; $\mu = 0.15$

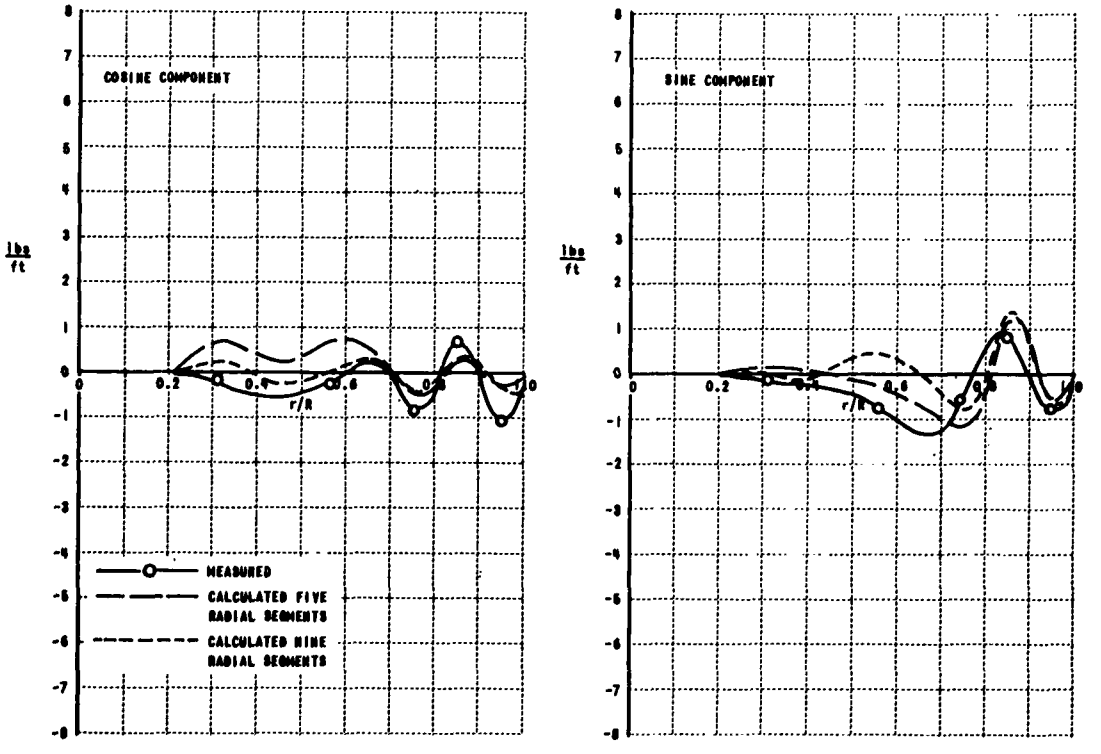

Figure 4l. 11th HARMONIC AIRLOADS; NASA MODEL; $\mu = 0.15$

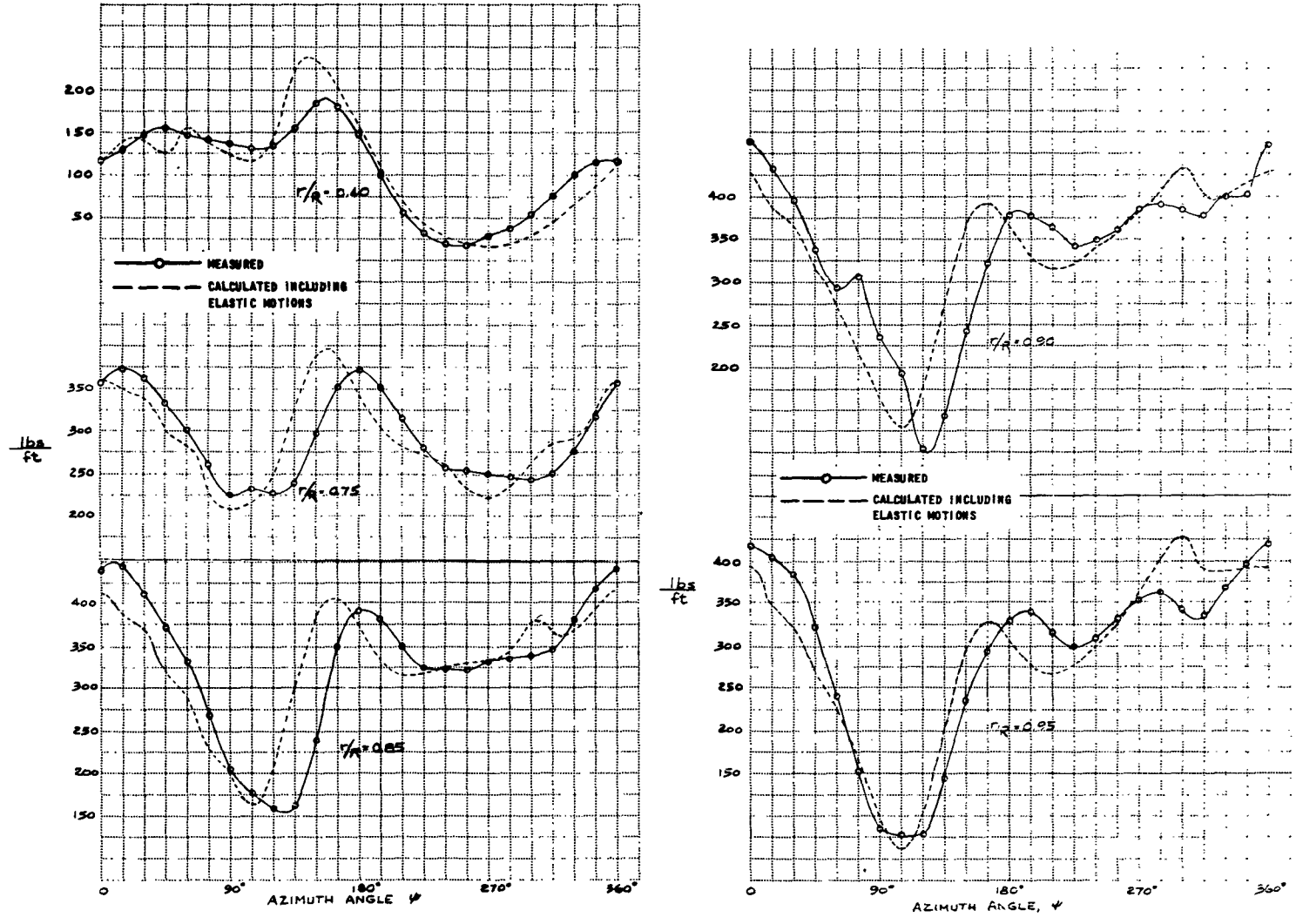

Figure 5. AZIMUTHAL VARIATION OF AIRLOADS FOR HU-1A; $\mu = 0.26$

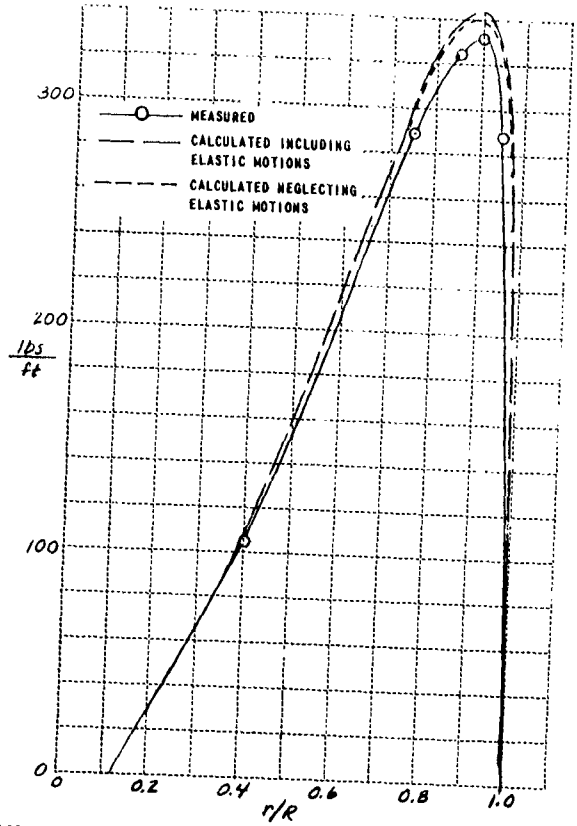

Figure 6. SPANWISE DISTRIBUTIONS OF THE HARMONICS OF THE MEASURED AND COMPUTED AIRLOADS
(a). ZEROTH HARMONIC (STEADY) AIRLOADS; HU-1A; $\mu = 0.26$

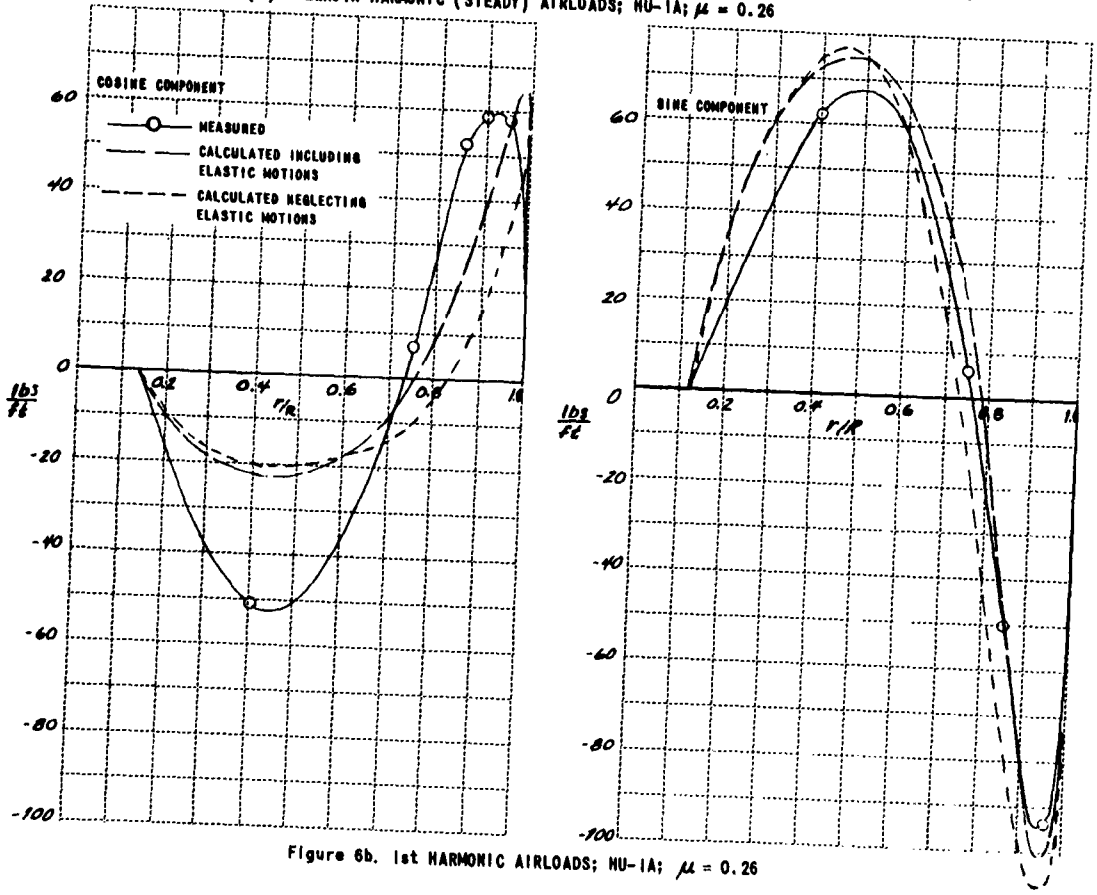

Figure 6b. 1st HARMONIC AIRLOADS; HU-1A; $\mu = 0.26$

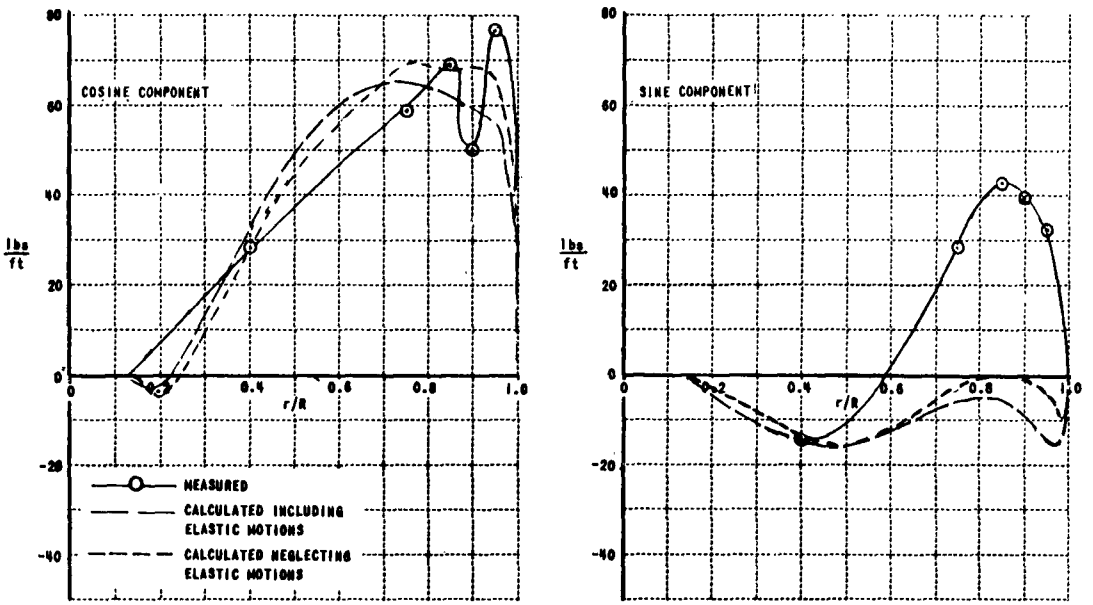

Figure 6c. 2nd HARMONIC AIRLOADS; HU-1A; μ = 0.2

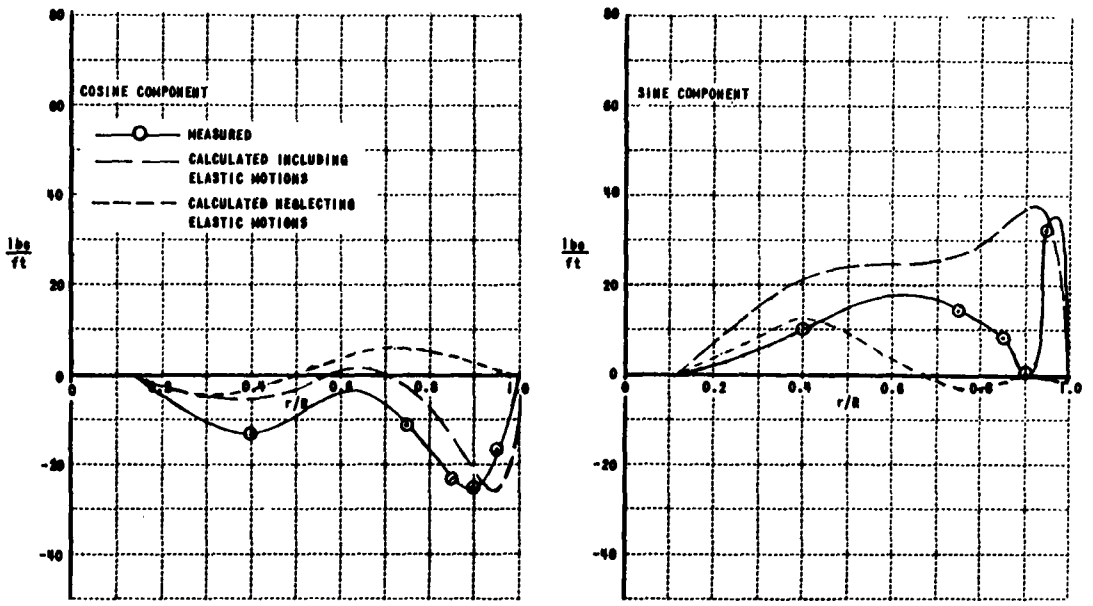

Figure 6d. 3rd HARMONIC AIRLOADS; HU-1A; μ = 0.26

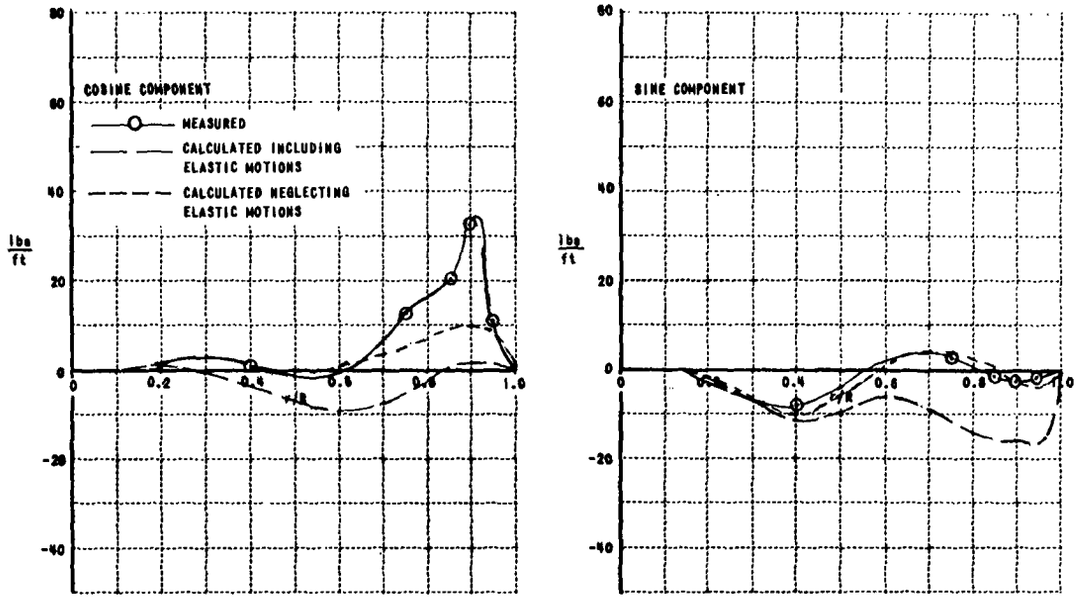

Figure 6e. 4th HARMONIC AIRLOADS; HU-1A; μ = 0.26.

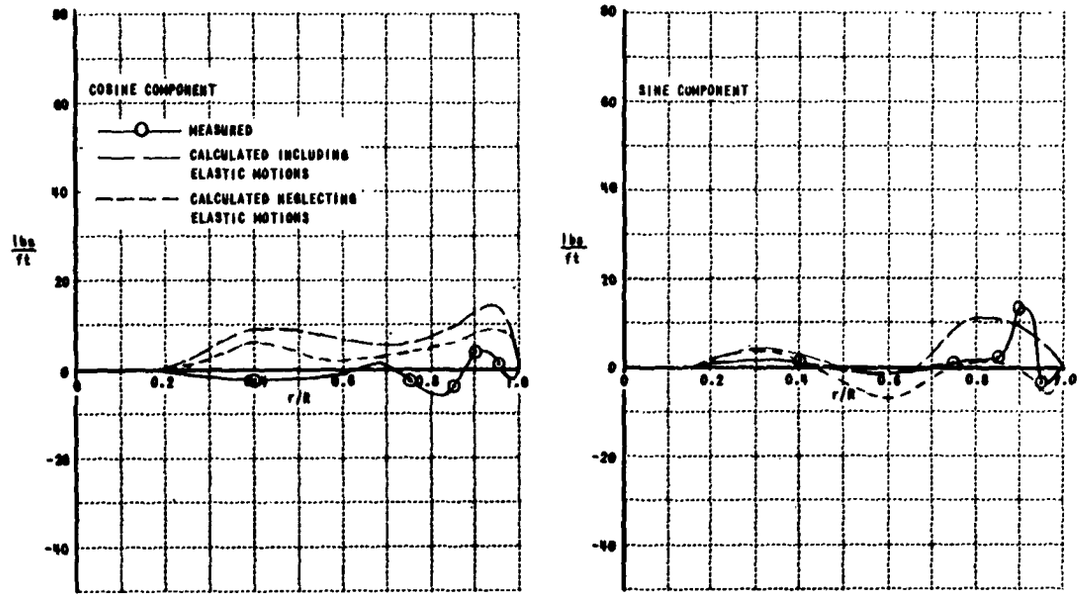

Figure 6f. 5th HARMONIC AIRLOADS; HU-1A; μ = 0.26

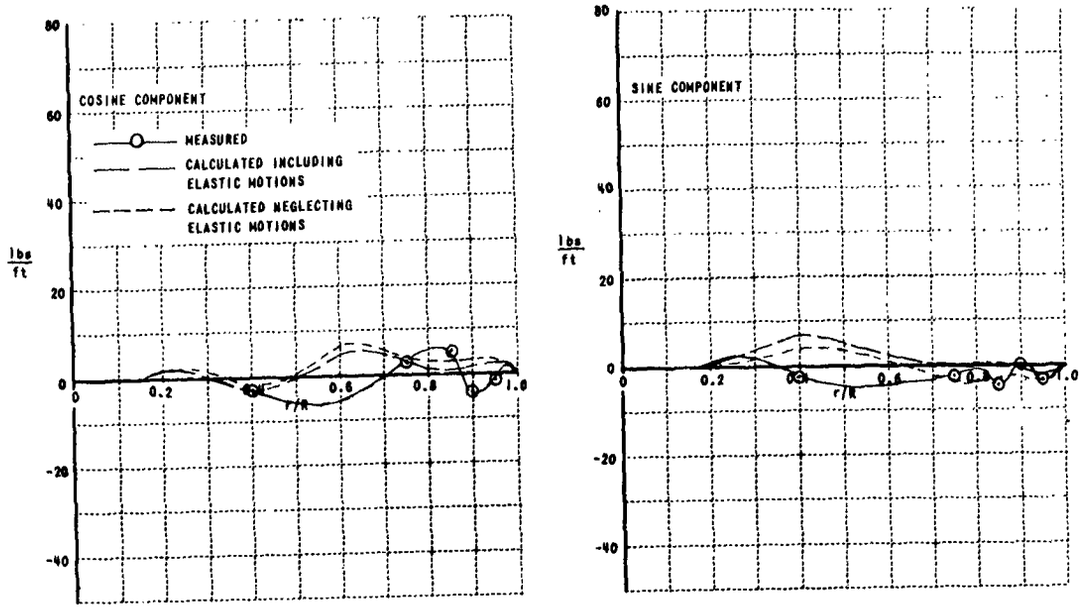

Figure 6g. 6th HARMONIC AIRLOADS; HU-1A; μ = 0.26

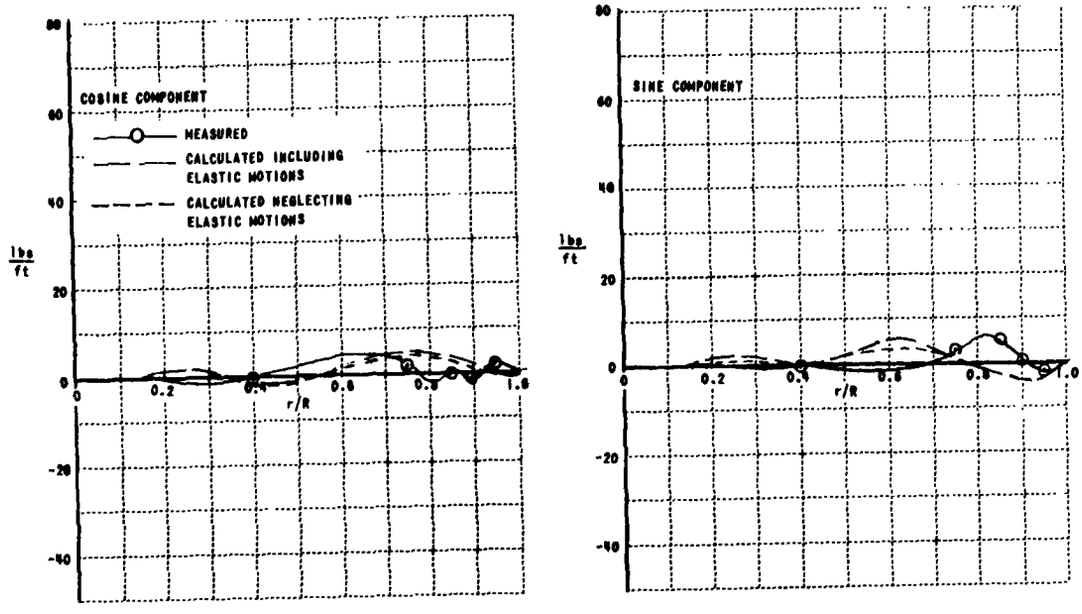

Figure 6h. 7th HARMONIC AIRLOADS; HU-1A; μ = 0.26

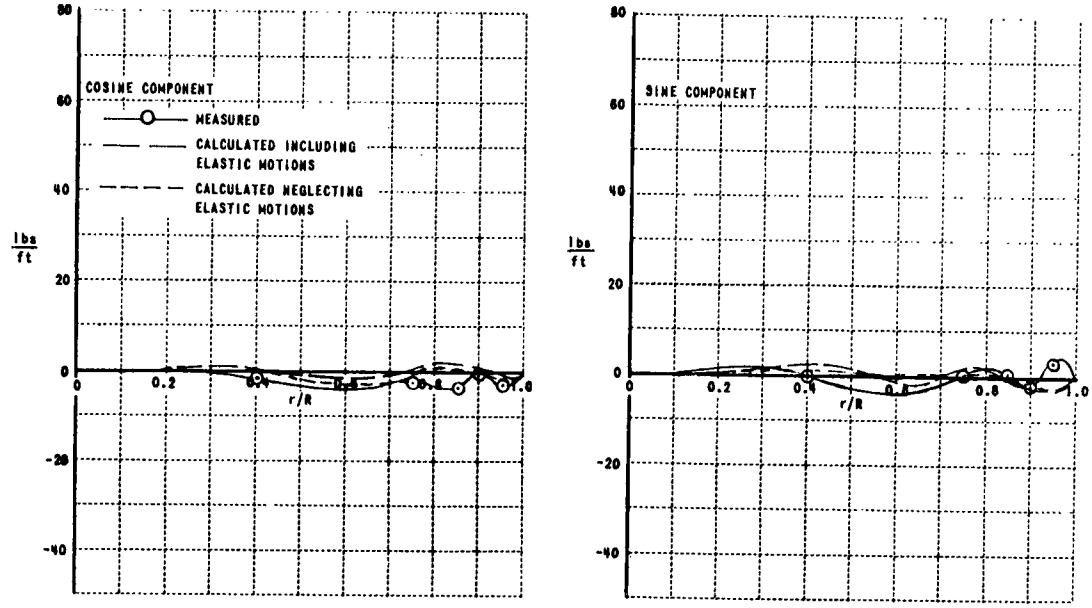

Figure 6i. 8th HARMONIC AIRLOADS; HU-1A; μ = 0.26

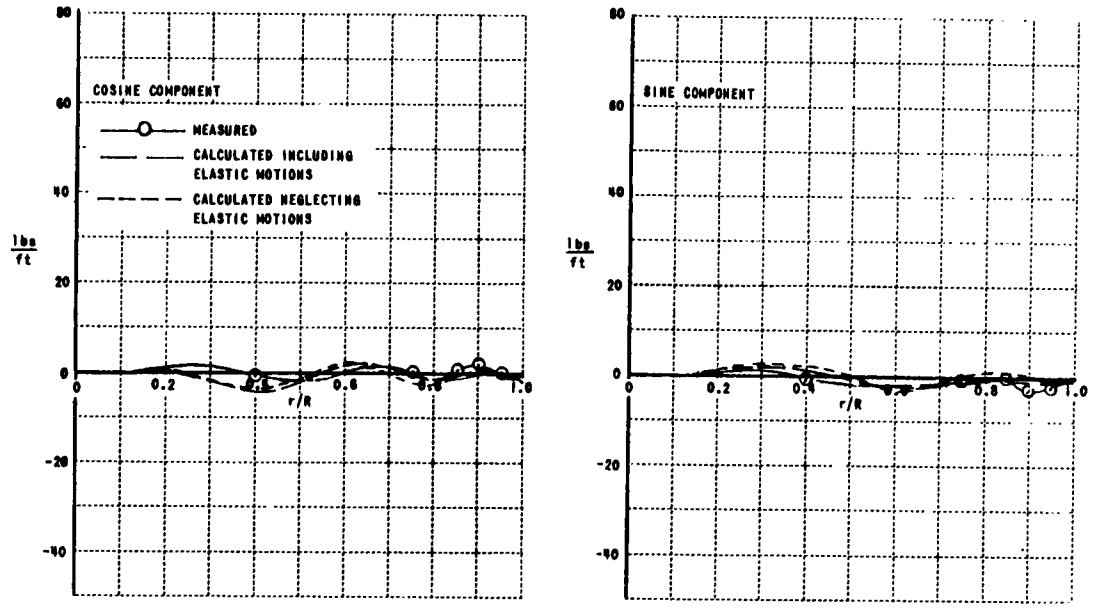

Figure 6j. 9th HARMONIC AIRLOADS; HU-1A; μ = 0.26

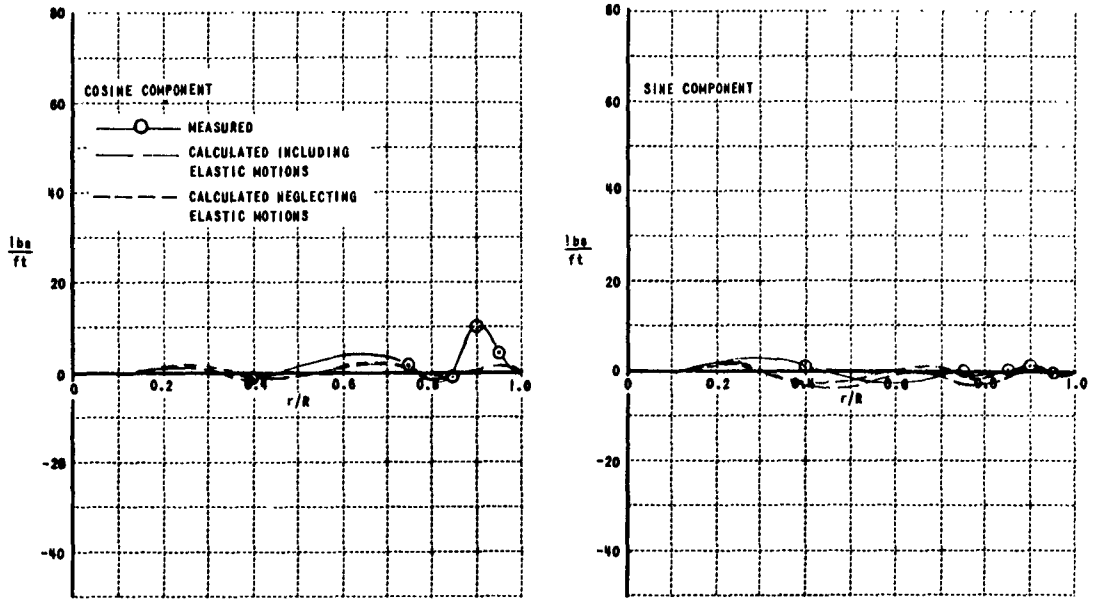

Figure 6k. 10th HARMONIC AIRLOADS; HU-1A; μ = 0.26

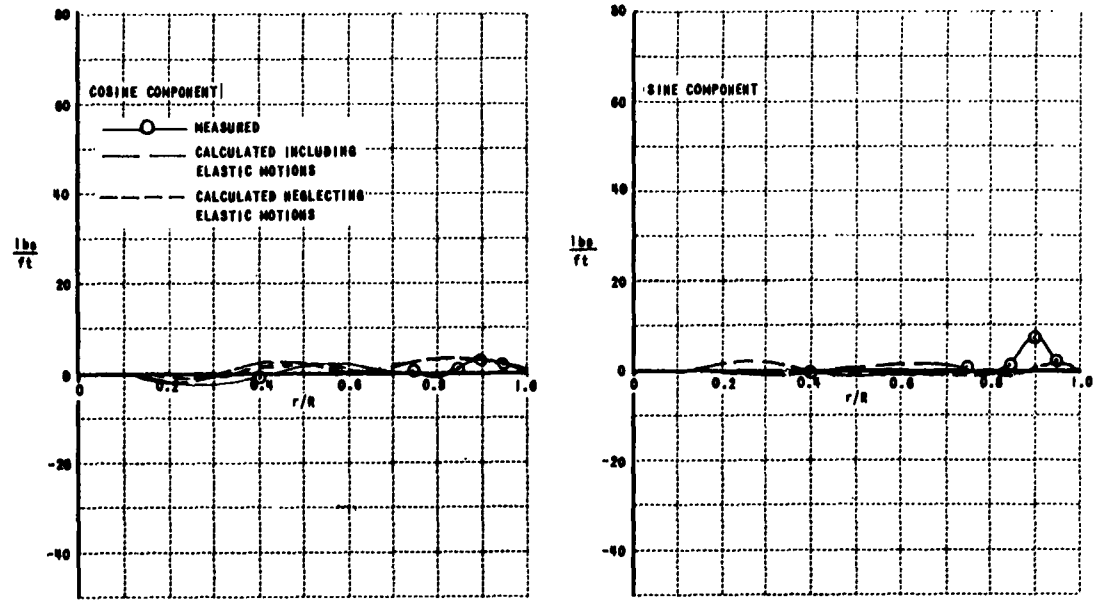

Figure 6l. 11th HARMONIC AIRLOADS; HU-1A; μ = 0.26

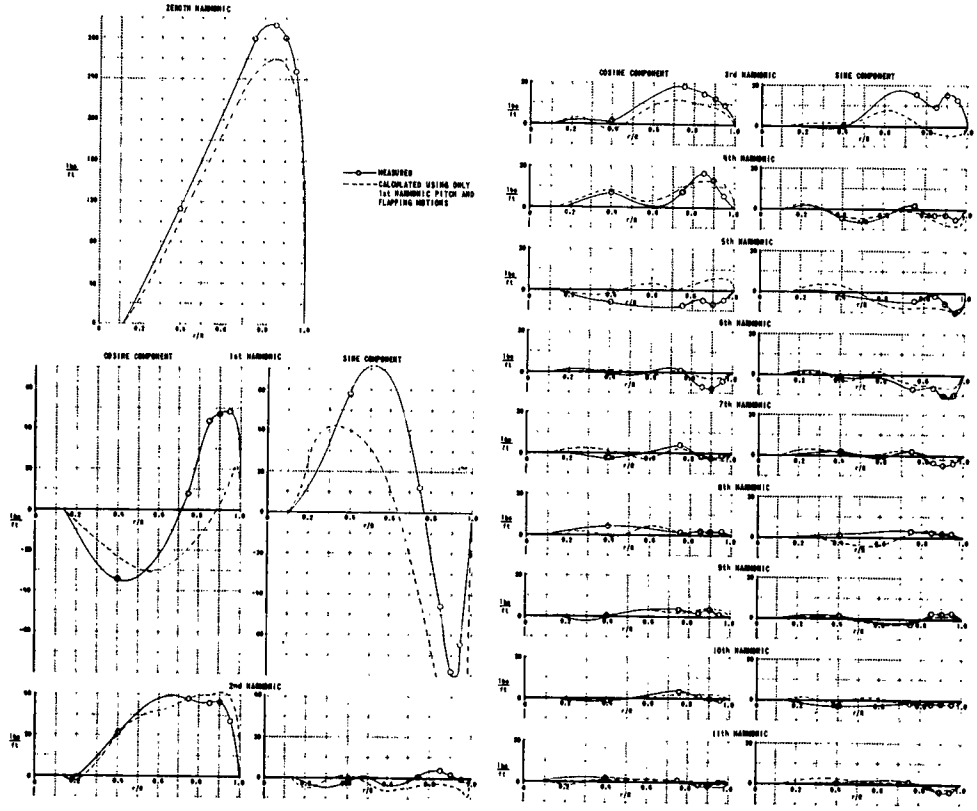

Figure 7. SPANWISE DISTRIBUTIONS OF THE HARMONICS OF THE MEASURED AND COMPUTED AIRLOADS FOR THE HU-1A; $\mu = 0.21$

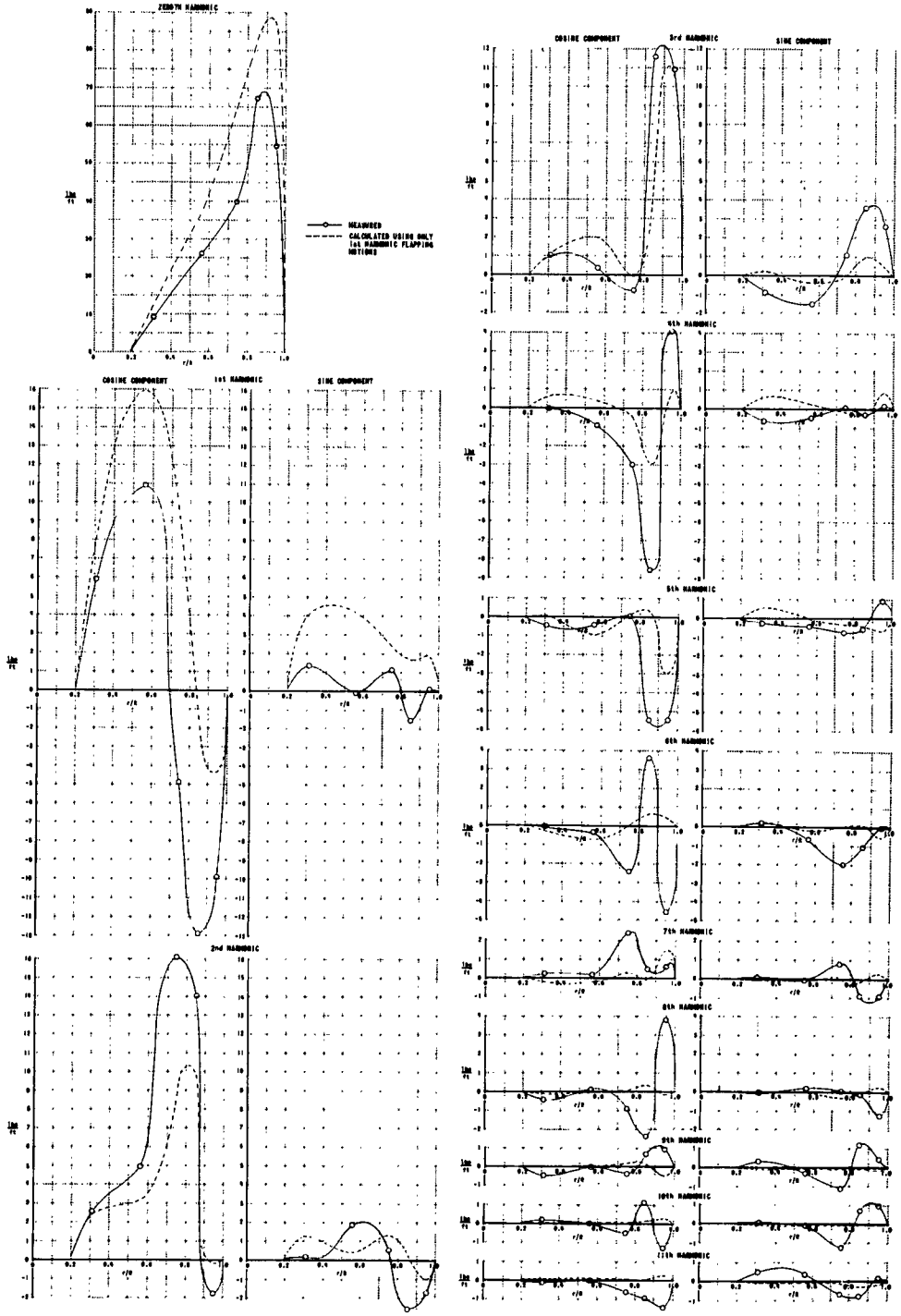

Figure 8. SPANWISE DISTRIBUTIONS OF THE HARMONICS OF THE MEASURED AND COMPUTED AIRLOADS FOR THE NASA MODEL ROTOR; μ = 0.08

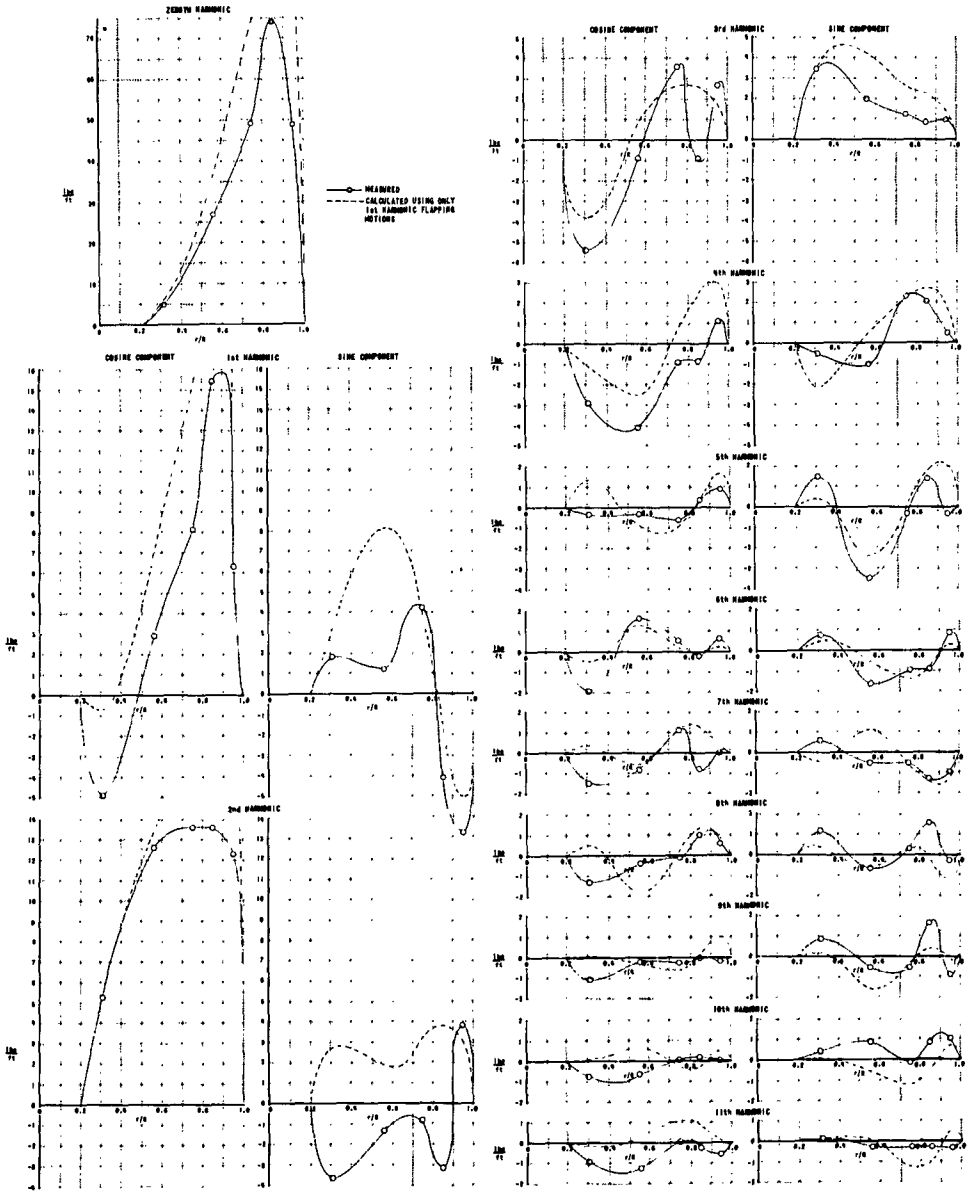

Figure 9. SPANWISE DISTRIBUTIONS OF THE HARMONICS OF THE MEASURED AND COMPUTED AIRLOADS FOR THE NASA MODEL ROTOR; $\mu = 0.29$

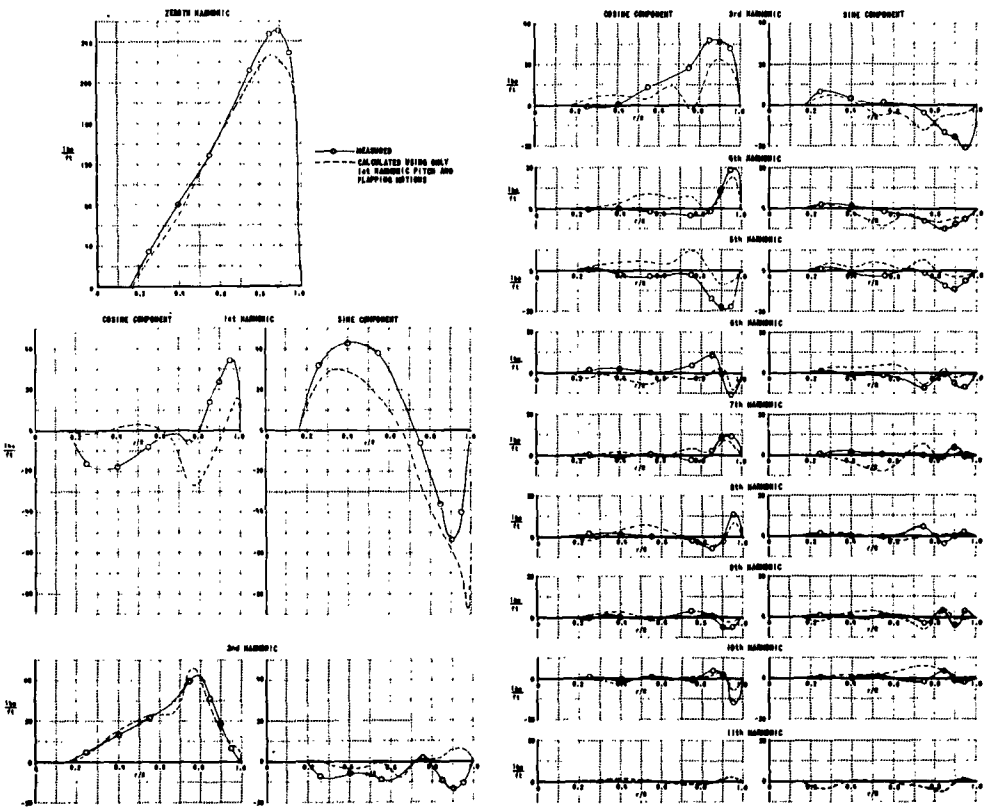

Figure 10. SPANWISE DISTRIBUTIONS OF THE HARMONICS OF THE MEASURED AND COMPUTED AIRLOADS FOR THE H-34; μ = 0.18

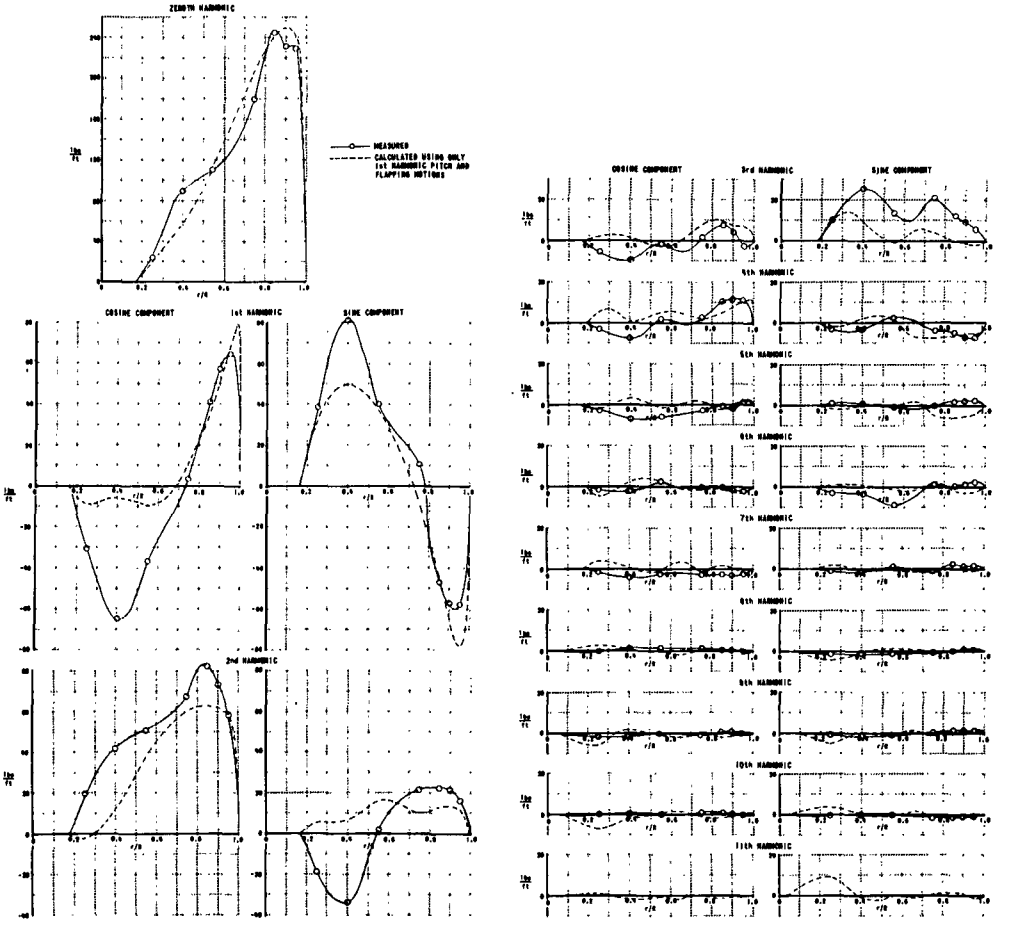

Figure 11. SPANWISE DISTRIBUTIONS OF THE HARMONICS OF THE MEASURED AND COMPUTED AIRLOADS FOR THE H-34; μ = 0.29

DISTRIBUTION

USAAVNBD	1
USATMC(FTZAT), ATO	1
OCRD, DA	1
NATC	1
CofT	2
USATMC	1
USATRECOM	60
USATRECOM LO, USARDG (EUR)	2
AFSC (Aero Sys Div)	2
CNR	2
BUWEPS, DN	2
USASGCA	1
Canadian LO, USATSCH	3
USASG, UK	1
NAFEC	3
Langley Research Center, NASA	2
Geo. C. Marshall Sp Flt Cen, NASA	1
MSC, NASA	1
NASA, Washington, D. C.	6
Ames Research Center, NASA	2
Lewis Research Center, NASA	1

Sci & Tech Info Fac	1
ASTIA	10
OUSRAMA	1
David Taylor Model Basin	1
Cornell Aeronautical Laboratory, Inc.	10
MOCOM	3

Cornell Aeronautical Laboratory, Inc., Buffalo, New York, A METHOD FOR COMPUTING ROTARY WING AIRLOAD DISTRIBUTIONS IN FORWARD FLIGHT - Raymond A. Piziali and Frank A. DuWaldt, TCREC Technical Rept 62-44, November 1962, 66 pp. (Contract DA 44-177-TC-698) USATRECOM Task 9R38-01-019-04.

Unclassified Report

A solution to the airloads problem for a rotating wing in steady-state translational flight is obtained. A sufficient amount of the wake detail

1. Rotary Wing Airload Prediction (Forward Flight)

Cornell Aeronautical Laboratory, Inc., Buffalo, New York, A METHOD FOR COMPUTING ROTARY WING AIRLOAD DISTRIBUTIONS IN FORWARD FLIGHT - Raymond A. Piziali and Frank A. DuWaldt, TCREC Technical Rept 62-44, November 1962, 66 pp. (Contract DA 44-177-TC-698) USATRECOM Task 9R38-01-019-04.

Unclassified Report

A solution to the airloads problem for a rotating wing in steady-state translational flight is obtained. A sufficient amount of the wake detail

1. Rotary Wing Airload Prediction (Forward Flight)

Cornell Aeronautical Laboratory, Inc., Buffalo, New York, A METHOD FOR COMPUTING ROTARY WING AIRLOAD DISTRIBUTIONS IN FORWARD FLIGHT - Raymond A. Piziali and Frank A. DuWaldt, TCREC Technical Rept 62-44, November 1962, 66 pp. (Contract DA 44-177-TC-698) USATRECOM Task 9R38-01-019-04.

Unclassified Report

A solution to the airloads problem for a rotating wing in steady-state translational flight is obtained. A sufficient amount of the wake detail

1. Rotary Wing Airload Prediction (Forward Flight)

Cornell Aeronautical Laboratory, Inc., Buffalo, New York, A METHOD FOR COMPUTING ROTARY WING AIRLOAD DISTRIBUTIONS IN FORWARD FLIGHT - Raymond A. Piziali and Frank A. Duwaldt, TCREC Technical Rept 62-44, November 1962, 66 pp. (Contract DA 44-177-TC-698) USATRECOM Task 9R38-01-019-04.

Unclassified Report

A solution to the airloads problem for a rotating wing in steady-state translational flight is obtained. A sufficient amount of the wake detail

was retained to enable accurate computation of the wake-induced velocities at the blades and, thus, the airload distribution.

The method developed is used to compute the airload distribution for several rotors for which measured and computed airloads are compared. In general, the agreement is quite good.

was retained to enable accurate computation of the wake-induced velocities at the blades and, thus, the airload distribution.

The method developed is used to compute the airload distribution for several rotors for which measured and computed airloads are compared. In general, the agreement is quite good.

was retained to enable accurate computation of the wake-induced velocities at the blades and, thus, the airload distribution.

The method developed is used to compute the airload distribution for several rotors for which measured and computed airloads are compared. In general, the agreement is quite good.

was retained to enable accurate computation of the wake-induced velocities at the blades and, thus, the airload distribution.

The method developed is used to compute the airload distribution for several rotors for which measured and computed airloads are compared. In general, the agreement is quite good.